A PROTECTIVE LANGERHANS CELL-KERATINOCYTE AXIS THAT IS DYSFUNCTIONAL IN PHOTOSENSITIVITY

A Dissertation

Presented to the Faculty of the Weill Cornell Graduate School

of Medical Sciences

in Partial Fulfillment of the Requirements for the Degree of

Doctor of Philosophy

by

William D. Shipman, III

May 2018

A PROTECTIVE LANGERHANS CELL-KERATINOCYTE AXIS THAT IS DYSFUNCTIONAL IN PHOTOSENSITIVITY

William D. Shipman III, Ph.D.

Cornell University 2018

Photosensitivity, or skin sensitivity to ultraviolet radiation (UVR), is a feature of lupus erythematosus (LE) and other autoimmune and dermatologic conditions, but the mechanistic underpinnings are poorly understood. Here, we identify a Langerhans cell (LC)-keratinocyte axis that limits UVR-induced keratinocyte apoptosis and skin injury via keratinocyte epidermal growth factor receptor (EGFR) stimulation. We show that the absence of LCs in Langerin-DTA mice leads to photosensitivity and that, in vitro, mouse and human LCs can directly protect keratinocytes from UVR-induced apoptosis. LCs express EGFR ligands and ADAM17, the metalloprotease that cleaves and activates EGFR ligands. Deletion of ADAM17 from LCs leads to photosensitivity and UVR induces LC ADAM17 activation and generation of soluble active EGFR ligands, suggesting that LCs protect by providing activated EGFR ligands to keratinocytes. Photosensitive systemic LE (SLE) models and human SLE skin show reduced epidermal EGFR phosphorylation and LC defects, and topical EGFR ligand reduces photosensitivity. Together, our data establish a direct tissue-protective function for LCs, reveal a mechanistic basis for photosensitivity, and suggest EGFR stimulation as a treatment for photosensitivity in LE and potentially other autoimmune and dermatologic conditions.

BIOGRAPHICAL SKETCH

William D. Shipman, III is from Whiteville, North Carolina and attended Morehouse College in Atlanta, GA where he earned a Bachelor of Science in Biology in 2010, graduating summa cum laude and with Phi Beta Kappa honors. As an undergraduate, he participated in the MBRS-RISE program, conducting research in the laboratory of Dr. Lawrence Blumer. During his undergraduate years, William also conducted research with the United States Environmental Protection Agency (EPA) and at the University of Buenos Aires. In 2010 William matriculated into the Weill Cornell/Rockefeller/Sloan-Kettering Tri-Institutional MD-PhD Program, and joined the laboratory of Theresa Lu, MD PhD in 2012. During his time in the laboratory, William has remained active in several community organizations at Weill Cornell Medicine and in New York City.

This dissertation is dedicated to my mother, Linda Daniels, and to my father, the late William D. Shipman Jr.

ACKNOWLEDGEMENTS

There are many people that contributed to my success as a graduate student and to the completion of this dissertation project. I would like to thank the Tri-Institutional MD-PhD Program, the Weill Cornell Medicine Immunology and Microbial Pathogenesis (IMP) Program, and the Hospital for Special Surgery Research Institute for administrative and scientific support as well as for providing a scientific community that is enriching and academically challenging.

I would like to thank Dr. Olaf Andersen, Dr. Ruthie Gotian, Renee Horton, and all the staff in the Tri-Institutional MD-PhD Program for being present and responsive to all of my needs as a student- both academic and non-academic. I would like to thank my thesis committee members: Dr. Carl Blobel, Dr. Richard Granstein, Dr. Michelle Lowes, Dr. Alessandra Pernis, and Dr. Jane Salmon for invaluable insight and guidance on this thesis project throughout the years.

Specifically related to this dissertation project, I would like to thank Susan Chyou, Anusha Ramanathan, Sneh Sharma, Dragos Dasoveanu for assistance in performing experiments; Tania Pannellinni and Cynthia Magro for assistance with interpreting experiments; Daniel Kaplan, Jane Salmon, Xioaping Qing, Eric Pamer, Babak Mehrara, James Young, Peter Izmirly, Robert Clancy, Richard Granstein, Michelle Lowes, and Carl Blobel for

providing reagents and critical intellectual input. I would also like to thank the laboratories of Inez Rogatsky and Alessandra Pernis for helpful discussions and reagents. My gratitude is also extended to all the members of the Lu Lab, both past and present. This work was supported by the funding sources: NIH MSTP T32GM007739 to the Weill Cornell/Rockefeller/Sloan-Kettering Tri-Institutional MD-PhD Program and NIH T32AR071302-01 to the HSS Research Institute Rheumatology Training program.

I would like to thank Theresa Lu, my thesis advisor, for her guidance and mentorship throughout my time as a graduate student. She has trained me to be a good and hardworking scientist and has worked tirelessly for the success of this dissertation project and of me as a graduate student. I am extremely appreciative of her believing in me and giving me a chance sometimes during challenging circumstances.

Finally, I would like to thank all of my family and friends for their support and encouragement during these challenging years as a graduate student. My family has remained extremely proud of me from the very beginning and that has encouraged me to continue to work hard. My sincerest love and gratitude is also extended to my partner Gabriel for being my companion, best friend, colleague, and supporter even during my most annoying days and long hours in lab. He and our dog Crumbs have kept me smiling and happy every day during this process.

TABLE OF CONTENTS

Biographical Sketch	iii
Dedication	iv
Acknowledgements	v
Table of Contents	vii
List of Figures	viii
List of Illustrations	x
Chapter I: Introduction	1
Chapter II: LCs limit UVR-induced keratinocyte apoptosis and skin injury via EGFR signaling	15
Chapter III: Characterization of a dysfunctional LC-keratinocyte axis in photosensitivity	49
Chapter IV: Discussion and Perspectives	64
Chapter V: Materials and Methods	75
References	90

LIST OF FIGURES

Figure 1. Characterization of Langerhans cells (LCs) in mouse and human skin 13

Figure 2. LCs limit keratinocyte apoptosis and skin inflammation at 24 hours after UVR exposure 14

Figure 3. LCs limit keratinocyte apoptosis and skin inflammation with UVA exposure alone 17

Figure 4. LCs limit UVR-induced skin injury at 5 days after UVR 18

Figure 5. LCs limit lesion development after multiple exposures of UVR 19

Figure 6. The role of accumulated monocytes and monocyte-derived DCs in UVR-induced skin injury 21

Figure 7. LCs limit UVR-induced keratinocyte apoptosis directly 23

Figure 8. Validation of phosphoEGFR Western blots and characterization of mouse epidermal EGFR expression 26

Figure 9. Mice treated with EGFR inhibitor resemble Langerin-DTA mice after UVR exposure 28

Figure 10. LCs are required for UVR-induced epidermal EGFR activation 30

Figure 11. EGFR ligand supplementation rescues the Langerin-DTA phenotype and human LCs protect keratinocytes similar to EGFR ligands 31

Figure 12. LCs protect keratinocytes by stimulating keratinocyte EGFR 32

Figure 13. Murine and human LCs express EGFR ligands and *Adam17* 35

Figure 14. LC-derived ADAM17 is important for limiting UVR-induced keratinocyte apoptosis and skin injury 36

Figure 15. Inducible deletion of ADAM17 in LCs results in increased UVR-induced keratinocyte apoptosis and skin inflammation 38

Figure 16. EGFR ligand supplementation rescues the phenotype of LC-Ad17 mice 39

Figure 17. ADAM17 deficient LCs are unable to protect keratinocytes from UVR-induced apoptosis 41

Figure 18. UVR directly activates LC ADAM17 43

Figure 19. UVR directly induces LC derived EGFR ligand release 44

Figure 20. MRL-*Fas*^{lpr} mice have a dysfunctional LC-keratinocyte axis 48

Figure 21. MRL-*Fas*^{lpr} LCs show no UVR-induced ADAM17 activation and EGFR ligand release and are unable to limit UVR-induced keratinocyte apoptosis 51

Figure 22. B6.Sle1Yaa mice are photosensitive 52

Figure 23. A dysfunctional LC-keratinocyte axis exists in B6.Sle1Yaa mice 55

Figure 24. A dysfunctional LC-keratinocyte axis exists in human SLE 57

Figure 25. Topical EGFR ligand reduces photosensitivity in in MRL-*Fas*^{lpr} mice 59

Figure 26. Topical EGFR ligand reduces draining lymph node B cell responses in MRL-*Fas*^{lpr} mice 61

Figure 27. Model of protective LC-keratinocyte axis and dysfunction of this axis in LE photosensitivity 63

LIST OF ILLUSTRATIONS

Illustration 1. Structure and cellular components of mouse and human skin 6

Illustration 2. Signaling pathways regulated by EGFR 12

CHAPTER I: INTRODUCTION

Systemic Lupus Erythematosus

Systemic lupus erythematosus (SLE) is a multifactorial autoimmune disease in which the host's immune system produces autoantibodies which in turn attack host cells and tissues. This results in a variety of symptoms and manifestations including joint pain and swelling, nephritis, skin inflammation, fever, lung damage, nervous system complications, and inflammation in other organs[1-3]. The incidence of SLE in the general population varies based on several different parameters including age, sex, race, ethnicity, and national origin. In the United States, the incidence is reported to range from 2.0-7.6 cases/100,000 persons/year [4]. Striking sex differences are noted in the epidemiology of SLE with 78% of SLE patients being female and the female to male ratio of the disease being 9:1 [5,6]. There also appears to be an ethnic correlate to the epidemiology of SLE with incidence rates being 10 times higher in African-Americans than in Caucasians and with incidence rates of SLE also being much higher in Asian populations [6-8].

SLE is a very complex illness to study and manage partly because it can affect almost any organ system or tissue and affects patients in highly variable manners [1-3]. The American College of Rheumatology (ACR) has developed the Criteria for Classification of SLE as a guide for clinicians to use to accurately diagnose SLE. The classification is based on 11 criteria and patients are considered to have SLE if 4 or more of the 11 criteria are present,

serially or simultaneously, during any interval of observation [9-11]. The 11 criteria include: malar rash, discoid rash, photosensitivity, oral ulcers, nonerosive arthritis, pleuritis or pericarditis, renal disorder, neurologic disorder (seizures or psychosis), hematologic disorder (hemolytic anemia, leukopenia, lymphopenia, or thrombocytopenia), immunologic disorder (anti-DNA, anti-Sm, or antiphospholipid antibodies), and positive antinuclear antibody [9-11].

Many SLE patients experience mild to more serious flares of the disease, with periods of active symptoms and periods of quiescence or remission [12]. The exact causes for lupus flares are still poorly understood, but it is thought that many environmental triggers such as sunlight exposure, medication, or infection can lead to a SLE flare [12]. Further understanding of what triggers an SLE flare would better allow clinicians to predict when a flare will occur, prevent a flare from happening, and manage the symptoms of a flare.

Since SLE is a chronic autoimmune disease with multiorgan involvement and an unpredictable course [1-3], many different potential mechanisms of disease have been proposed and supported within the last decade. The various mechanisms of pathophysiology that have been used to describe the disease process of SLE include: genetic influences, epigenetic regulation, environmental factors, female hormones and sex, immune cells, and cytokines[1-3]. However, there is still a need for more understanding of the

disease pathogenesis of SLE and how these processes could potentially be modulated.

Cutaneous manifestations of SLE

Cutaneous manifestations appear in 75-85% of patients with SLE and represent the first sign of disease in 23-28% of SLE patients [13]. The classification of skin lesions in lupus erythematosus (LE) are considered to be either LE-specific or LE-nonspecific, primarily by histological analysis [14]. LE non-specific manifestations, which are cutaneous lesions or inflammatory conditions that are commonly associated with SLE but are also found in other diseases, include: vascular skin changes (e.g. periungual telangiectasia, livedo racemosa, thrombophlebitis, Raynaud's phenomenon, and acral occlusive vasculopathy); leukocytoclastic vasculitis (which can occur as palpable purpura or urticarial vasculitis, especially hypocomplementemic urticarial vasculitis); papular mucinosis; calcinosis cutis; non-scarring alopecia; and erythema multiforme [15].

Separately from SLE, patients may also be diagnosed with cutaneous specific LE or cutaneous lupus erythematosus (CLE) where the primary findings of the disease are related to skin manifestations [16]. LE-specific cutaneous findings encompass the established subtypes of CLE (Dusseldorf classifications): acute CLE (ACLE); subacute CLE (SCLE); chronic CLE (CLE)- discoid LE (DLE), Chilblain LE (CHLE), or LE profundus/panniculitus

(LEP); intermittent CLE (ICLE); and LE tumidus (LET) [15,17,18]. Classification of individual subtypes is based on clinical presentation and histological findings.

Photosensitivity in SLE

Photosensitivity, a sensitivity to ultraviolet radiation (UVR) whereby even ambient sunlight exposure can result in inflammatory skin lesions, is a common feature in SLE and CLE and can also occur with other autoimmune conditions, a number of dermatologic conditions, and as a response to drugs such as fluoroquinolone antibiotics [19,20,21] . The photosensitive lesions can be disfiguring and, in SLE, can be associated with systemic disease flares. It was discovered that SLE patients who were exposed to artificial tanning sources (a source of UVR) demonstrated marked exacerbation of SLE disease activity with increased antinuclear antibody titers, proteinuria, and polyarthalgia [22]. Another study conducted in 2007 described the onset of a severe case of lupus nephritis and the detection of high serum levels of anti-dsDNA and anti-Ro/SSA antibodies in a patient who was previously in complete remission of SLE but had recent extended exposure to sunlight [23]. Much of the data describing how UVR or sunlight exposure can lead to flares in systemic SLE are anecdotal in nature but widely accepted, so more work is needed to fully characterize this phenomenon.

The pathogenesis of photosensitivity is poorly understood and treatments consist mainly of sun avoidance and sunscreen to prevent lesion

development [20]. A better understanding of the mechanistic basis of photosensitivity could lead to improved disease treatment. Many investigations suggest that the pathophysiology of photosensitivity involves: impaired clearance of apoptotic cells in the skin, UVR-induced chemokine production, and/or UVR-induced enhancement of cellular adhesion molecules [21,24-26].

Keratinocyte apoptosis occurs rapidly following UVR exposure, and photosensitivity is associated with increased keratinocyte apoptosis [25,27]. In autoimmune diseases, apoptotic keratinocytes can display autoantigens that bind autoantibodies, leading to complement activation and sustained skin inflammation [19 ,25]. The localization of "sunburn cells," or apoptotic keratinocytes, with LE skin lesions [28] further supports the idea that keratinocyte apoptosis is part of the pathophysiology of photosensitivity. Keratinocytes are critical for normal skin barrier function [29], and, even in the absence of autoimmunity, increased keratinocyte death and failure to compensate has the potential to lead to skin injury and inflammation [30] . However, mechanisms that limit UVR-induced keratinocyte apoptosis that are dysfunctional in photosensitivity are not well understood.

Langerhans cells

The skin consists of an epidermal, dermal, and subdermal layer that contains various immune cells and stromal structures that are necessary for the appropriate functioning of the skin (Illustration 1 [31]). Various types of skin-

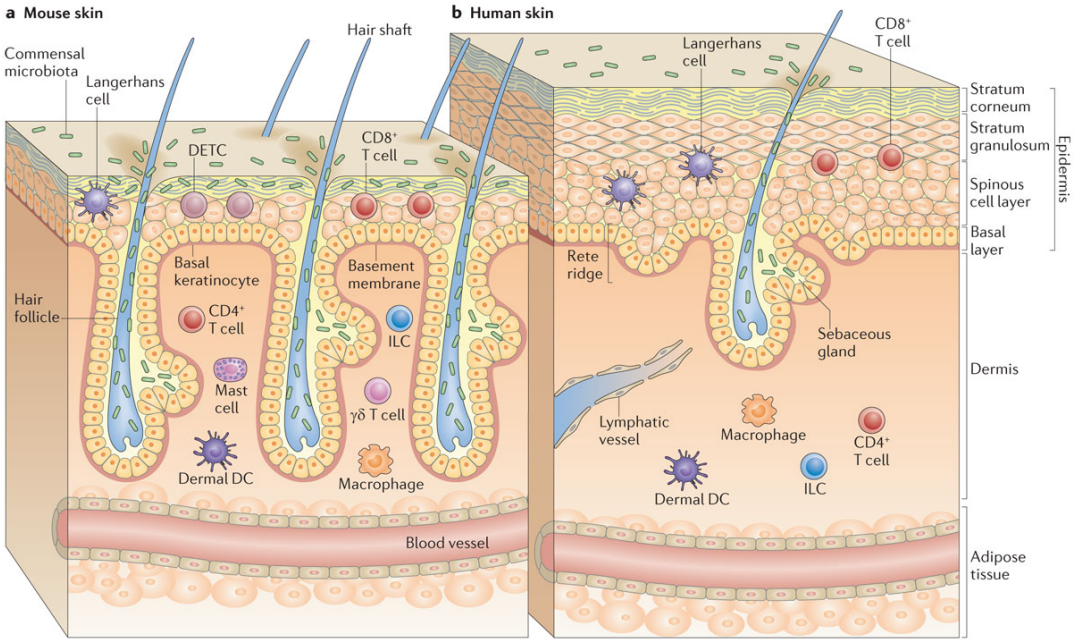

Illustration 1. Structure and cellular components of mouse and human skin. (A) Mouse skin. **(B)** Human skin. DETC: dendritic epidermal T cell, DC: dendritic cell, ILC: innate lymphoid cell [31].

associated immune cells have been implicated in the pathogenesis of cutaneous manifestations of SLE and CLE including T cells, plasmacytoid dendritic cells (pDCs), natural killer cells (NK cells), and Langerhans cells (LCs)[25,32]. In particular dendritic cells (DCs) have received attention for the role that they play in the pathophysiology of CLE. DCs were first discovered in 1973 by Ralph Steinman[33] and have since been found to function as important antigen presenting cells by capturing and processing antigens in the periphery, expressing lymphocyte co-stimulatory molecules, migration to lymphoid organs, and secreting cytokines to initiate immune responses- essentially serving as a vital link between the innate and adaptive immune responses[33,34].

In recent years it has been debated as to whether LCs are to be classified as DCs or as macrophages. LCs have the ability to present antigens like DCs but they are similar to macrophages in ontogeny[35]. LCs are primarily associated with their antigen presentation functions: capturing antigens in the epidermis, migrating from the skin to the draining lymph node, and initiating T cell responses[35,36]. However, LCs can also have regulatory roles, regulating T cell priming in contact hypersensitivity [37] and promoting regulatory T cell generation [38]. LCs can also regulate intrinsic NK cell phenotype and NK cell-mediated skin inflammation independent of antigen presentation to T cells[39]. The various roles that LCs play in regulating other immune processes will be interesting to understand in the future.

LCs have been implicated in the pathogenesis of cutaneous manifestations of LE but a clear understanding of the role of LCs in LE is still needed. In 1982,Sontheimer and Bergstresser demonstrated that LCs in patients with CLE were less dendritic in morphology, irregularly distributed in the epidermis, and present in decreased numbers when compared to LCs in adjacent normal skin[45]. In this study, the authors utilized nonlesional and lesional skin biopsies from patients with 3 different types of CLE (SCLE-papulosquamous, SCLE-annular, and DLE) and by whole mount epidermal sheet processing, were able to illustrate LCs in lesional skin appearing irregular. While LCs in the nonlesional epidermal sheets were regularly and evenly distributed with primary, secondary, and tertiary dendrites (typical of normal LC morphology[19,28]) LCs in lesional epidermal sheets were abnormally rounded with few or no dendrites present[40]. ATPase, the surface marker enzyme used to stain the LCs in this experiment, was decreased in intensity on LCs in the lesional epidermal sheets when compared to nonlesional epidermal sheets, suggesting a decrease in ATPase activity in lesional LCs. LCs in nonlesional epidermal sheets were evenly and monotonously distributed, while LCs in lesional epidermal sheets were irregularly distributed with some areas even completely devoid of LCs and with abnormal, very large, elongated LCs occasionally appearing[45]. Since the morphology and dendritic structure of LCs may play a key role in their function and viability, these data suggest that LCs may perhaps be dysfunctional in LE skin or perhaps behaving abnormally.

In addition to LC morphology and distribution, Sonthemier and Bergstresser also made another interesting observation: that LCs were found in significantly lower cell densities in CLE lesional epidermal sheets when compared to CLE nonlesional skin[45]. In order to differentiate this disparity in LC morphology and density found in CLE lesional skin with other inflammatory skin disorders, similar experiments were conducted in patients with dermatomyositis and lichen planus. Interestingly, LCs appeared increased in number in lichen planus and exhibited similar morphological alterations to CLE lesional skin in dermatomyositis. However, LCs in dermatomyositis were found to have persevered epidermal densities and distributions[45]. These comparisons with lichen planus and dermatomyositis suggest that perhaps the morphological alteration, decrease in epidermal LC density, and irregular distribution is unique to LCs in CLE.

This study also attempted to assess the function of LCs in lesional CLE by examining the allogeneic lymphocyte stimulating capacity of CLE epidermal cells. Interestingly, lesional LCs from CLE patients were just as efficient in stimulating lymphocytes as LCs from nonlesional skin[45], suggesting that the alloantigen presenting capacity of these LCs is preserved. However, since the role that LCs play in the pathogenesis of CLE lesions or other skin manifestations of CLE may not be related to their ability to present antigen, these findings do not negate the potential pivotal role of LCs in LE-associated skin inflammation.

Later Mori et al. not only discovered similar findings regarding LCs in CLE lesions but extended the current knowledge with the implementation of electron microscopy. Upon analysis with electron microscopy, epidermal LCs in lesional CLE skin appeared depleted of organelles in addition to dendrites and contained tubuloreticular inclusions while dermal DCs (CD11c+ CD14+ cells) were found localized around capillaries in the papillary dermis[46]. In addition, epidermal LCs from lesional CLE skin were found to have lower levels of HLA-DR antigen as compared with nonlesional skin. These data further suggested that the alterations in cytological differentiation and expression of significant molecules by epidermal LCs may represent an impairment in their function and a possible role in the pathogenesis of CLE.

EGFR and ADAM17 in the skin

Epidermal growth factor receptor (EGFR) is a member of the ErbB family of tyrosine kinase growth factor receptors. EGFR is a transmembrane protein (~180 kDa) with an extracellular domain that is capable of binding up to seven known ligands including epidermal growth factor (EGF), heparin-binding EGF-like growth factor (HB-EGF), amphiregulin, epiregulin, transforming growth factor α (TGFα), betacellulin, and epigen[41-43]. Once a ligand binds to the extracellular portion of EGFR, receptor dimerization occurs which triggers autophosphorylation of tyrosine residues in the carboxy terminus of EGFR. Subsequently, these phosphorylated tyrosine residues

serve as binding sites or “loading docks” for molecules containing Src homology 2 domains, which can then initiate a variety of cell signaling pathways[41] (Illustration 2 [44]). Activation of EGFR signaling is known to activate several cellular responses including angiogenesis, inhibition of apoptosis, DNA synthesis, cell proliferation, migration, adhesion, and survival[41-43].

A disintegrin and metalloprotease 17 (ADAM17) is a transmembrane matrix metalloprotease that is known to cleave and therefore activate membrane-bound EGFR ligands (except EGF and betacellulin) [45-50]. It is thought that most EGFR activation is due to soluble EGFR ligand binding [45], therefore, the role of ADAM17 is critical in EGFR signaling. One of the major functions of ADAM17 and other ADAM molecules is proteolytic processing or protein ectodomain shedding. Many cellular proteins are membrane-bound and require further post-translational processing before they are biologically active. This is where ADAM17 and other ADAM molecules become critical. ADAM17 has been shown to cleave EGFR ligands from the surface of the cell, allowing them to become soluble and activate EGFR on distant cells or the same cell [45,47,48]. Although it is possible that membrane tethered EGFR ligands can still activate EGFR on neighboring cells, ADAM17 knockout models suggest that paracrine signaling is important for EGFR activation and that EGFR ligands function primarily in their soluble form [45].

Previous studies have shown that EGFR is critical for maintaining keratinocyte survival specifically after UVR exposure. Epidermal EGFR (likely

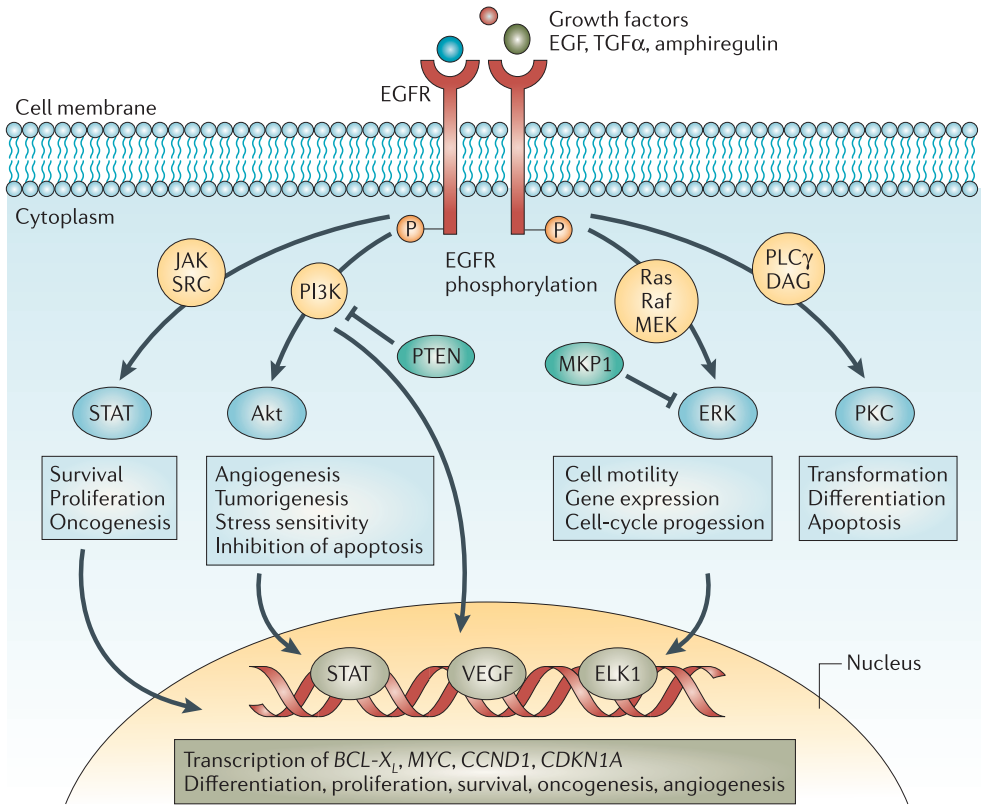

CCND1, gene encoding cyclin D1; *CDKN1A*, gene encoding p21; JAK, Janus kinase; TGFα, tranforming growth factor-α.

Illustration 2. Signaling pathways regulated by EGFR. EGFR phosphorylation can directly or indirectly activate signal transducer and activator of transcription 1 (STAT1), STAT3, and STAT5, which can then regulate gene expression responsible for cell survival, proliferation, and oncogenesis. EGFR signaling can also activate phosphatidylinositol 3-kinase (PI3K) than can initiate a signaling cascade that stimulate angiogenesis, tumorigenesis, stress sensitivity, and inhibition of apoptosis. The Ras, Raf, mitogen-activated protein kinase (MEK) pathway is also activated by EGFR and can induce cell motility, cell-cycle progression, and gene expression in general. Phospholipase c-γ (PLCγ) can also bind to phosphorylated EGFR and become activated, leading to the subsequent activation of diacylglycerol (DAG) and the activation of protein kinase-C (PKC), which can stimulation cell transformation, differentiation, and apoptosis. PTEN: phosphatase and tensin homolog, MKP1: mitogen-activated protein kinase phosphatase 1, ERK: extracellular signal-regulated kinase, VEGF: vascular endothelial growth factor [44].

representing primarily keratinocyte EGFR) is activated rapidly after UVR exposure [51,52], suggesting that EGFR likely plays a role in UVR-induced effects. El-Abaseri and colleagues showed that the inhibition of EGFR decreased UVR-induced keratinocyte proliferation and also increased UVR-induced apoptosis [51]. This group later showed that EGFR knockout skin grafts resulted in decreased UVR-induced epidermal hyperplasia and increased UVR-induced apoptosis [52], suggesting that EGFR is a major regulator of UVR-induced effects in the skin and that EGFR played a protective role for keratinocytes after UVR exposure by promoting their survival [42].

ADAM17 in keratinocytes has been shown to play important roles in epidermal homeostasis. Keratinocyte specific ADAM17 deletion (K14Cre-ADAM17$^{flox/flox}$ mice) results in homeostatic epidermal barrier defects including increased barrier permeability, increased transepidermal water loss (TEWL), and dysfunctional cornification of keratinocytes[53]. These mice also showed increased inflammatory cell infiltration, decreased EGFR activation (phosphorylated EGFR expression) and were phenotypically similar to EGFR knockout mice[53]. These data show that ADAM17-EGFR signaling in keratinocytes regulates keratinocyte health at homeostasis and regulates skin barrier integrity. However, the role of ADAM17 in neighboring immune cells of the epidermis and the role these cells play in EGFR signaling in keratinocytes is still poorly understood. In addition, the importance of keratinocyte ADAM17 under inflammatory conditions is still unknown.

We and others have recently shown that dendritic cells (DCs) can directly modulate stromal elements in lymph nodes, adipose tissues, and skin [54-58]. As LCs have DC characteristics[35,36], we asked whether LCs modulated keratinocyte survival and skin injury after UVR exposure. Here we delineate an LC-keratinocyte axis whereby LCs limit UVR-induced keratinocyte apoptosis and skin injury by activating keratinocyte EGFR. This axis is dysfunctional in photosensitive SLE mouse models and there is also evidence of dysfunction in human SLE. Photosensitivity in one of the SLE models is reduced by EGFR ligand supplementation. Together our results identify a tissue protective function for LCs, provide insight into mechanisms that limit skin injury, and suggest that EGFR stimulation may be an approach for treatment of photosensitivity in LE and other diseases.

CHAPTER II: LCs LIMIT UVR-INDUCED KERATINOCYTE APOPTOSIS AND SKIN INJURY VIA EGFR SIGNALING.

Keratinocyte apoptosis is a known feature of photosensitivity and is thought to contribute to the pathogenesis, but mechanisms that regulate keratinocyte apoptosis are still poorly understood. Since DCs in lymph node and adipose tissue regulate stromal cell survival [54,55], we asked if LCs play a role in maintaining keratinocyte survival and limiting UVR-induced skin injury.

LCs limit UVR-induced keratinocyte apoptosis and skin injury

LCs are positioned within the epidermis with keratinocytes in both mouse and human skin (Fig. 1A,B), suggesting that LCs have the potential to modulate UVR-induced keratinocyte apoptosis. To determine if LCs regulated UVR-induced keratinocyte apoptosis, we utilized the Langerin-DTA mouse model that is constitutively depleted of LCs (Fig. 1C) but not of Langerin+ dermal DCs [37]. We treated wild-type (WT) and Langerin-DTA mice with UVR and examined the skin at 24 hours (Fig. 2A). LCs were present but reduced by half with UVR (Fig. 1C), likely due to LC emigration [35,36] . As expected, UVR induced an increase in activated caspase-3+ cells in the epidermis (Fig. 2B, left). These cells were Langerin- (Fig. 2C) and CD3- (Fig. 2D), consistent with the idea that the apoptotic cells were keratinocytes. The lack of activated caspase-3+ Langerin+ cells also suggested that LCs were not ingesting apoptotic keratinocytes. Langerin-DTA mice showed more activated caspase-

Figure 1

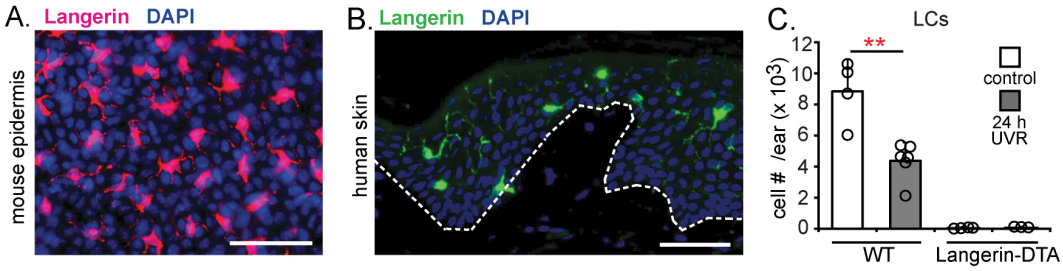

Figure 1. Characterization of Langerhans cells (LCs) in mouse and human skin. (A) Representative image of mouse epidermal whole mount stained with anti-Langerin (pink) and DAPI (blue) (n= 3). **(B)** Representative image of human skin stained with anti-Langerin (green) and DAPI (blue) (n= 3 healthy control human patients). Dashed line indicates epidermal-dermal junction. **(A,B)** Scale bar: 50 μm. **(C)** WT and Langerin-DTA mice were treated with UVR and ears examined at 24 hours and LC numbers were enumerated by flow cytometry (n= 3-6). Bars represent averages. Error bars depict standard deviation. **p<0.01 using two-tailed unpaired Student's t-test.

Figure 2. LCs limit keratinocyte apoptosis and skin inflammation at 24 hours after UVR exposure. (A-G) WT and Langerin-DTA mice were exposed to UVR and the ears from these mice and non-exposed control mice were examined 24 hours later. **(A)** Experimental scheme for **(B-G)**. **(B)** Activated caspase-3+ keratinocytes per high powered field (HPF). Left: Representative images of Langerin (red) and activated caspase-3 (green) stain. Right: Quantification (n= 3-9). Scale bars: 50 μm. **(C)** Activated caspase-3+ Langerin+ LC numbers in tissue sections (n= 3-9). **(D)** Activated caspase-3+ CD3+ T cell numbers (n= 3-4). **(E)** Activated caspase-3+ keratinocyte numbers at indicated time after UVR exposure (n= 1-4). **(F)** Absolute (left) and normalized (right) monocyte numbers assessed by flow cytometry (n= 3-7). **(G)** Absolute numbers of monocyte-derived DCs, CD11b+ DCs, CD11b- DCs, macrophages, and neutrophils (n= 3-7). **(B-G)** Bars represent averages. Error bars depict standard deviation

Figure 2

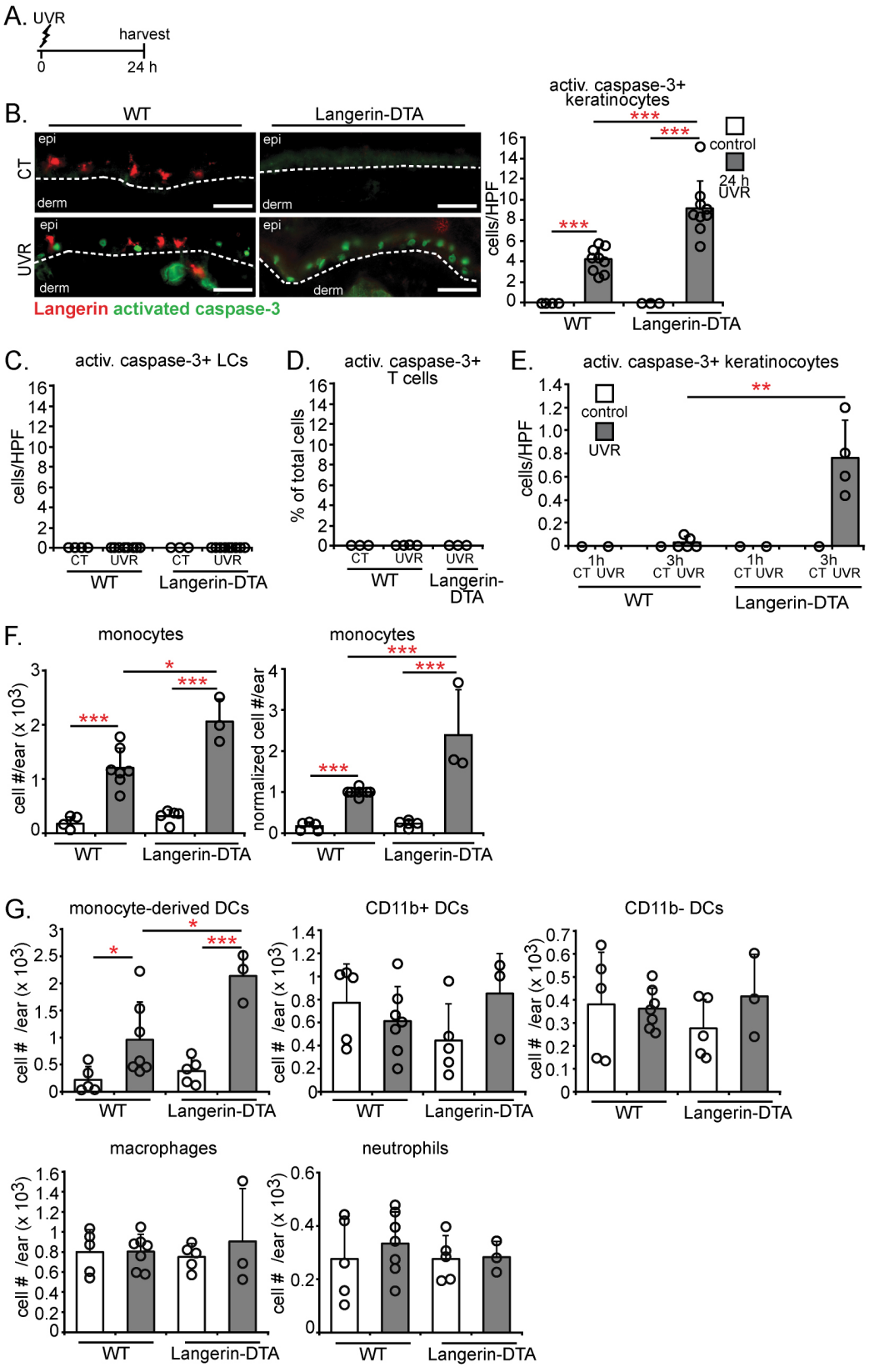
A.
UVR
harvest
0
24 h
B.
WT
Langerin-DTA
CT
UVR
epi
derm
Langerin activated caspase-3
activ. caspase-3+ keratinocytes
cells/HPF
control
24 h UVR
WT
Langerin-DTA
C.
activ. caspase-3+ LCs
cells/HPF
CT
UVR
WT
Langerin-DTA
D.
activ. caspase-3+ T cells
% of total cells
Langerin-DTA
E.
activ. caspase-3+ keratinocytes
cells/HPF
control
UVR
1h
3h
F.
monocytes
cell #/ear (x 10³)
normalized cell #/ear
G.
monocyte-derived DCs
CD11b+ DCs
CD11b- DCs
cell # /ear (x 10³)
macrophages
neutrophils

3+ keratinocytes relative to WT mice (Fig. 2B, right), and this occurred as early as 3 hours after UVR exposure (Fig. 2E). Langerin-DTA mice had greater monocyte accumulation (Fig. 2F). This was associated with greater numbers of monocyte-derived DCs (Fig. 2G), while CD11b- DCs, CD11b+ DCs, macrophages, and neutrophils did not increase in Langerin-DTA mice (Fig. 2G). Our UVR source provided both UVA and UVB [59], and greater effects of UVR on Langerin-DTA mice remained when UVB was blocked by use of a Mylar filter (Fig. 3A-C), suggesting that LCs limit the effects of at least UVA and likely also of UVB. Together, these results suggested that LCs limit UVR-induced keratinocyte apoptosis and skin inflammation.

We then assessed additional parameters of skin function. UVR induces epidermal hyperplasia in mice several days after exposure [52], likely as a compensatory mechanism, and Langerin-DTA mice showed less epidermal thickening than WT mice (Fig. 4A,B). Epidermal barrier function is compromised after UVR exposure despite the hyperplasia [60], and Langerin-DTA skin showed greater tissue penetrance of toluidine blue [53] than WT skin (Fig. 4C), suggesting worsened barrier function. Consistent with worsened skin function, Langerin-DTA mice showed a greater lesional area after exposure of shaved skin to multiple days of UVR (Fig. 5A-C). These results together suggested that LCs limit the extent of UVR-induced skin injury.

We next attempted to assess whether the monocytes that accumulated in UVR-treated skin contributed to the UVR-induced damage. Consistent with the work of Tamoutounour et al. [61], we could identify CCR2+ monocytes and

Figure 3

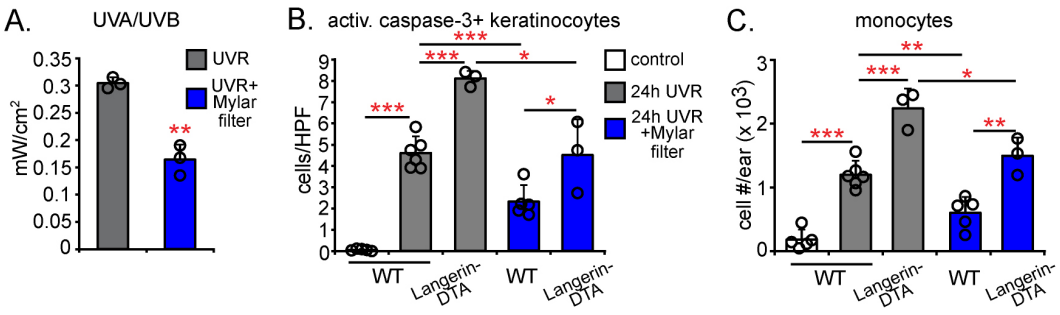

Figure 3. LCs limit keratinocyte apoptosis and skin inflammation with UVA exposure alone. (A) UVA/UVB measurements of UVR source without and with Mylar filter (n=3). Each symbol represents the value measured during independent experiments. **(B,C)** WT and Langerin-DTA mice were treated with UVR or UVR+Mylar filter and examined with non-exposed controls at 24 hours (n= 3-6). **(B)** Activated caspase-3+ keratinocyte numbers. **(C)** Absolute monocyte numbers. Bars represent average value and error bars depict standard deviation. *p<0.05, **p<0.01, ***p<0.001 using two-tailed unpaired Student's t-test.

Figure 4

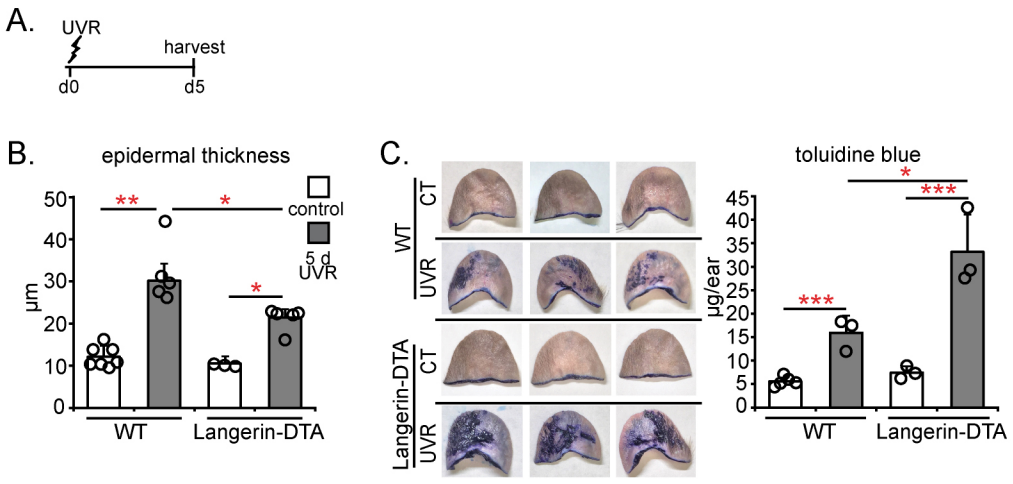

Figure 4. LCs limit UVR-induced skin injury at 5 days after UVR. (A) Experimental scheme for **(B,C)**; WT and Langerin-DTA mice were exposed to UVR and the ears from these mice and non-exposed control mice were examined 5 days after UVR exposure. **(B)** Epidermal thickness (n= 3-7). **(C)** Epidermal permeability as assessed by toluidine blue penetrance. Left: Representative images of toluidine blue treated ears. Right: Quantification (n= 3-5). Bars represent average value and error bars depict standard deviation. *p<0.05, **p<0.01, ***p<0.001 using two-tailed unpaired Student's t-test.

Figure 5

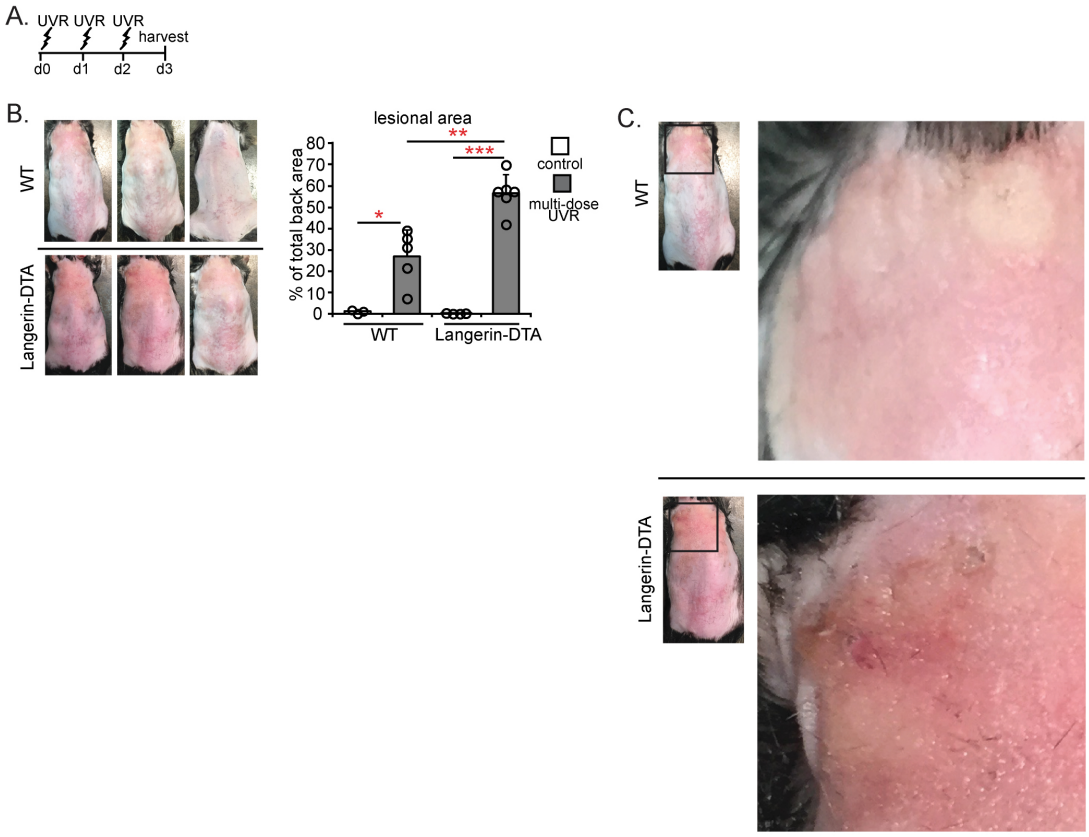

Figure 5. LCs limit lesion development after multiple exposures of UVR. **(A)** Experimental scheme for **(B)**; mice were exposed to UVR for 3 days and examined 24 hours after the final UVR exposure. **(B)** Left: Representative images of back skin. Right: Lesional area quantification (n= 3-5). **(C)** Magnified images of back skin lesions from Fig. 5B. **(B)** Bars represent average value and error bars depict standard deviation. *p<0.05, **p<0.01, ***p<0.001 using two-tailed unpaired Student's t-test.

monocyte-derived DCs in inflamed skin and CD11b+ DCs were also CCR2+ (Fig. 6A). Monocytes and monocyte-derived DCs comprised the vast majority of CCR2+ cells (Fig. 6B). LCs were CCR2- (Fig. 6C). We depleted the CCR2+ cells using CCR2-DTR mice (Fig. 6D)[62]. The depletion did not alter UVR-induced keratinocyte apoptosis or epidermal thickness (Fig. 6E,F) but reduced toluidine blue penetrance (Fig. 6G). Although we cannot rule out a role for the CD11b+ DCs, these data raise the possibility that greater levels of infiltrating monocytes and monocyte-derived cells contributed to the worsened barrier function in Langerin-DTA mice.

LCs directly protect keratinocytes

T cells also inhabit the epidermis [36] (Fig. 7A) and we asked whether LCs limited UVR-induced skin inflammation and injury via T cells. Rag1-/-Langerin-DTA mice lacking both lymphocytes and LCs showed higher UVR-induced keratinocyte apoptosis than Rag1-/- mice (Fig. 7B). While Rag1-/- mice showed higher UVR-induced monocyte accumulation than WT mice (Fig. 7C), Rag1-/-Langerin-DTA mice showed even greater monocyte accumulation (Fig. 7C). These results suggested that LC-mediated skin protection was independent of antigen presentation to T cells and that LCs could potentially limit keratinocyte apoptosis directly.

To test for direct LC-keratinocyte interactions, we performed LC-keratinocyte co-cultures. UVR induces keratinocyte apoptosis in vitro [63], and addition of LCs reduced the apoptosis (Fig. 7D,E). Essentially no activated

Figure 6. **The role of accumulated monocytes and monocyte-derived DCs in UVR-induced skin injury**. **(A-C)** CCR2-GFP reporter mice were exposed to UVR and ears were examined at indicated time points along with a B6 staining control (n=3). **(A)** Flow cytometry gating strategy for CCR2+ populations in the skin using the scheme of Tamoutounour et al.[61] Lineage= B220, CD3, Ly6G, and pan-NK CD49b **(B)** Percentage of CCR2+ cells in the skin that are monocytes, monocyte-derived DCs, and CD11b+ DCs. **(C)** Representative histograms of CCR2-GFP expression in LCs as assessed by flow cytometry (n= 3). **(D-G)** WT and CCR2-DTR mice were injected with PBS or 250ng DT at d-1 and d0 of UVR exposure and examined 24 hours later with non-exposed control mice (n= 3) **(E),** or injected with PBS or DT at d-1, d0, and d3 of UVR exposure and examined 5 days later with non-exposed control mice (n= 3-4) **(D,F,G)**. **(D)** Monocyte, monocyte-derived DC, and CD11b+ DC depletion at 5 days after UVR exposure. **(E)** Activated caspase-3+ keratinocyte numbers. **(F)** Epidermal thickness. **(G)** Epidermal permeability. Left: Representative images of toluidine blue penetrance. Right: Quantification. **(B,D-G)** Each symbol represents 1 mouse**.** Data from 2 **(A-C,E)** and 3 **(D,F,G)** independent experiments. Bars represent average value and error bars depict standard deviation. n.s.= not significant $p>0.05$,**$p<0.01$, ***$p<0.001$ using two-tailed unpaired Student's t-test.

Figure 6

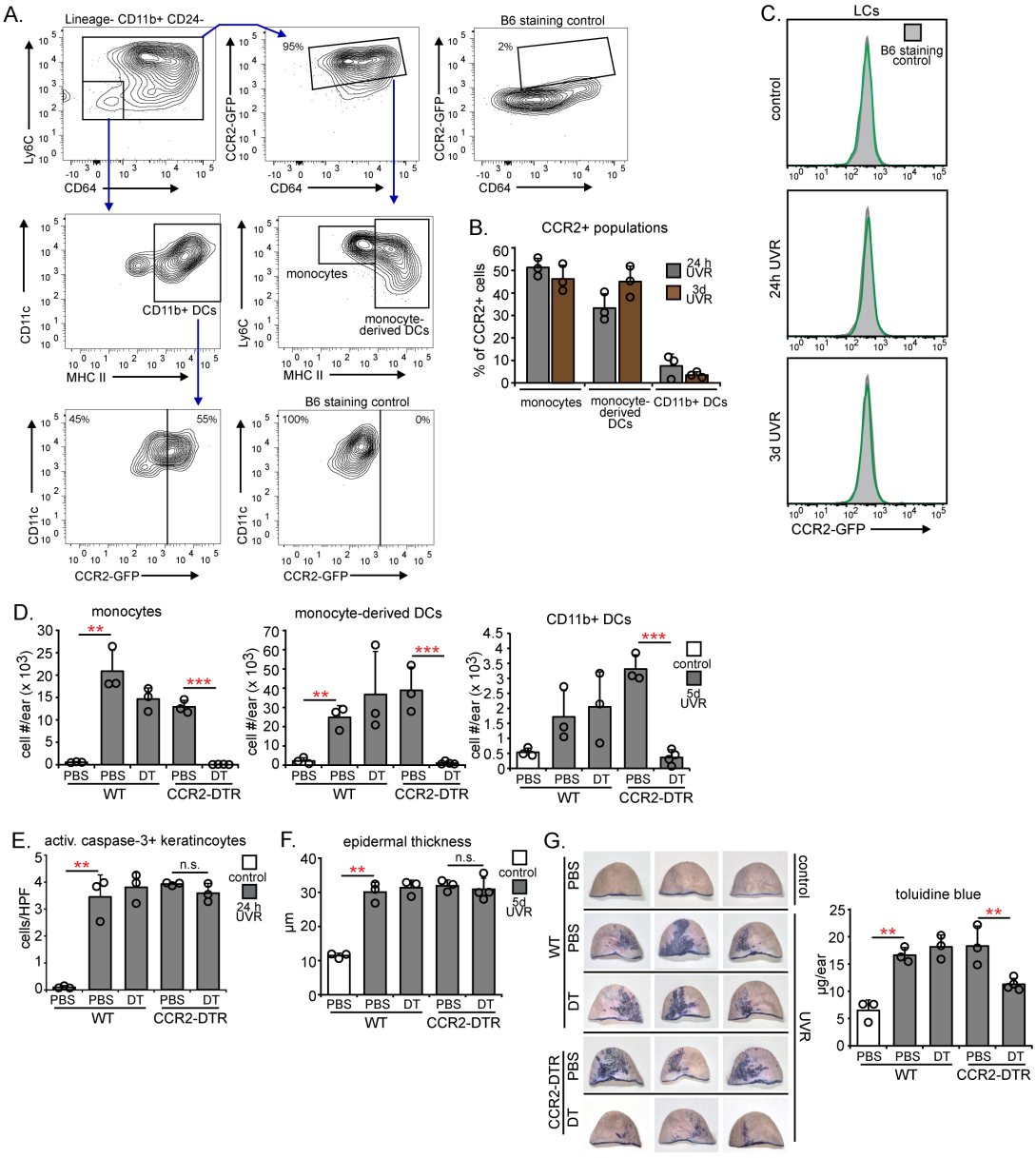
A.
Lineage- CD11b+ CD24-
Ly6C
CD64
CCR2-GFP
95%
B6 staining control
2%
CD11c
CD11b+ DCs
monocytes
monocyte-derived DCs
MHC II
45%
55%
100%
0%
B.
CCR2+ populations
% of CCR2+ cells
24 h UVR
3d UVR
monocytes
monocyte-derived DCs
CD11b+ DCs
C.
LCs
B6 staining control
control
24h UVR
3d UVR
CCR2-GFP
D.
monocytes
monocyte-derived DCs
CD11b+ DCs
cell #/ear (x 10³)
PBS
DT
WT
CCR2-DTR
control
5d UVR
E.
activ. caspase-3+ keratincoytes
cells/HPF
n.s.
24 h UVR
F.
epidermal thickness
µm
5d UVR
G.
control
UVR
WT
CCR2-DTR
toluidine blue
µg/ear

Figure 7. LCs limit UVR-induced keratinocyte apoptosis directly. (A) Mouse epidermis whole-mount stain for CD3 (red), Langerin (green), and DAPI (blue). **(B,C)** Rag1-/-, Rag1-/-Langerin-DTA, WT, and Langerin-DTA mice were exposed to UVR and ears were harvested 24 hours later (n= 3-8). **(B)** Activated caspase-3+ keratinocytes. **(C)** Absolute (left) and normalized (right) monocyte numbers. **(D,E)** Effect of LCs on keratinocyte survival in vitro. Murine keratinocyte cultures without and with LCs were exposed to UVR (n= 3). **(D)** Representative images of cultures stained for Langerin (green), activated caspase-3 (red), and DAPI (blue). **(E)** Activated caspase-3+ keratinocytes. **(F)** Activated caspase-3+ cells that were Langerin+ (LCs) (n= 3). **(G)** LC-mediated protection of keratinocytes in the absence of phenol red. Murine keratinocyte cultures without and with LCs were exposed to UVR in phenol red-containing media (used for most experiments) or phenol red-free keratinocyte growth media and activated caspase-3+ keratinocyte numbers were quantified (n= 3). **(A, D)** Scale bars: 50 μm. **(B,C,E-G)** Bars represent averages. Error bars depict standard deviation. *$p<0.05$, **$p<0.01$, ***$p<0.001$ using two-tailed unpaired Student's t-test.

Figure 7

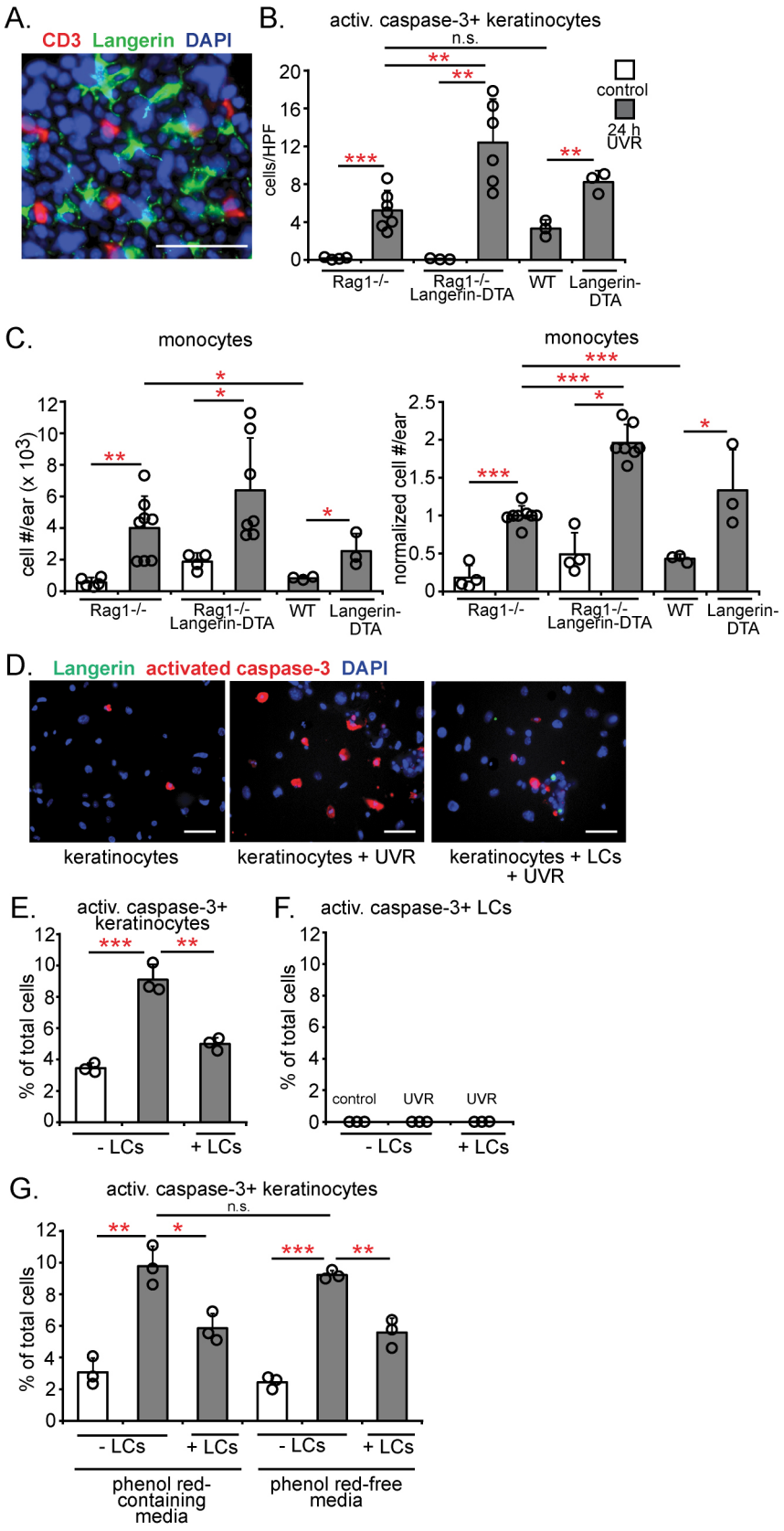
A.
CD3 Langerin DAPI
B.
activ. caspase-3+ keratinocytes
n.s.
**
**
***
**
control
24 h UVR
cells/HPF
20
16
12
8
4
0
Rag1-/-
Rag1-/- Langerin-DTA
WT
Langerin-DTA
C.
monocytes
*
*
**
*
cell #/ear (x 10^3)
12
10
8
6
4
2
0
Rag1-/-
Rag1-/- Langerin-DTA
WT
Langerin-DTA
monocytes
***
***
*
***
*
normalized cell #/ear
2.5
2
1.5
1
0.5
0
Rag1-/-
Rag1-/- Langerin-DTA
WT
Langerin-DTA
D.
Langerin activated caspase-3 DAPI
keratinocytes
keratinocytes + UVR
keratinocytes + LCs + UVR
E.
activ. caspase-3+ keratinocytes
***
**
% of total cells
12
10
8
6
4
2
0
- LCs
+ LCs
F.
activ. caspase-3+ LCs
% of total cells
12
10
8
6
4
2
0
control
UVR
UVR
- LCs
+ LCs
G.
activ. caspase-3+ keratinocytes
n.s.
**
*
***
**
% of total cells
12
10
8
6
4
2
0
- LCs
+ LCs
- LCs
+ LCs
phenol red-containing media
phenol red-free media

caspase-3+ cells were Langerin+ (Fig. 7F), suggesting that the reduction in apoptotic keratinocytes with the addition of LCs was not due to ingestion and clearance of apoptotic keratinocytes. These effects were not due to phototoxicity from the phenol red-containing culture medium as the results were similar in phenol red-free medium (Fig. 7G). Together, these results suggested that LCs limit UVR-induced keratinocyte apoptosis and skin injury in vivo by direct interactions with keratinocytes.

LCs limit UVR-induced keratinocyte apoptosis and skin injury by stimulating epidermal EGFR

As keratinocyte EGFR signaling protects against UVR-induced keratinocyte apoptosis [52,64] and plays an important role in maintaining epidermal barrier function and limiting skin inflammation [29,65], we hypothesized that the LC-mediated protection of skin involved EGFR signaling. Treatment of WT mice with PD168393, an irreversible EGFR inhibitor [66], reduced epidermal EGFR phosphorylation at tyrosine 1068, a residue associated with keratinocyte survival with UVR [64], as expected (Fig. 8A,B). Ninety-eight percent of epidermal EGFR+ cells were keratinocytes (Fig. 8C,D), suggesting that the epidermal EGFR phosphorylation in Western blots reflected mainly keratinocyte signaling. EGFR inhibition led to increased UVR-induced keratinocyte apoptosis and skin injury (Fig. 9A-D). This resembled the phenotype of Langerin-DTA mice, supporting the idea that LCs may limit UVR-induced skin injury by modulating keratinocyte EGFR signaling.

Figure 8. Validation of phosphoEGFR Western blots and characterization of mouse epidermal EGFR expression. (A) Mice were treated topically with 4mM EGFR inhibitor-PD168393 or vehicle prior to UVR exposure and examined 1 hour after UVR exposure. Representative Western blot of epidermal EGFR phosphorylation at 1 hour after UVR (n= 3). **(B)** Positive control for EGFR phosphorylation, showing effects of intradermally injected recombinant EGF (5μg) at 5 minutes (n= 2). **(C)** Flow cytometry gating strategy for total EGFR (tEGFR)+ cells in the epidermis. **(D)** Percent of tEGFR+ cells in each epidermal cell population examined (n= 4). Bars represent average value and error bars depict standard deviation. ***$p<0.001$ using two-tailed unpaired Student's t-test.

Figure 8

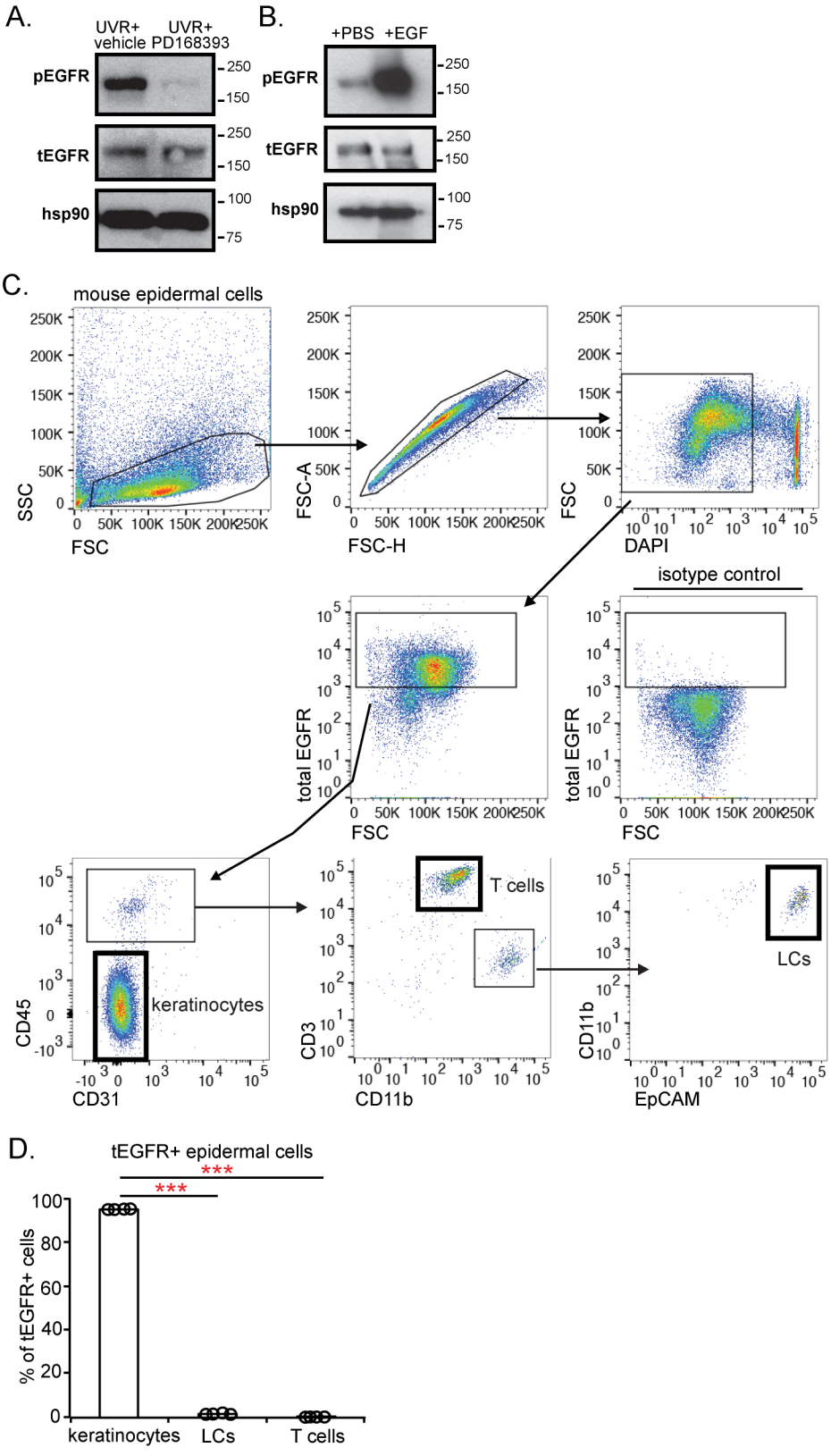
A.
UVR+ vehicle
UVR+ PD168393
pEGFR
tEGFR
hsp90
250
150
100
75
B.
+PBS
+EGF
pEGFR
tEGFR
hsp90
250
150
100
75
C.
mouse epidermal cells
SSC
FSC
FSC-A
FSC-H
FSC
DAPI
isotype control
total EGFR
FSC
CD45
CD31
keratinocytes
CD3
CD11b
T cells
CD11b
EpCAM
LCs
D.
tEGFR+ epidermal cells
***
***
% of tEGFR+ cells
keratinocytes
LCs
T cells

Figure 9

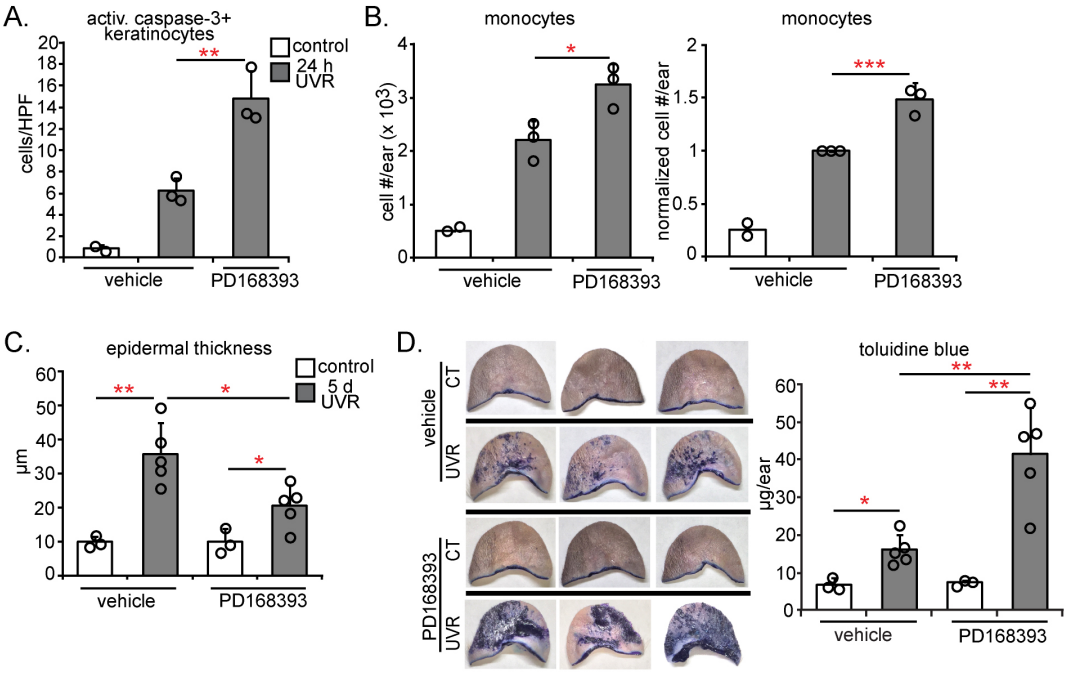

Figure 9. Mice treated with EGFR inhibitor resemble Langerin-DTA mice after UVR exposure. (A-D) Mice were treated topically with 4mM EGFR inhibitor-PD168393 or vehicle prior to UVR exposure and examined 24 hours **(A,B)** or 5 days after UVR exposure **(C,D)**. **(A)** Activated caspase-3+ keratinocyte numbers (n= 2-3). **(B)** Absolute (left) and normalized (right) monocyte numbers (n= 2-3) **(C)** Epidermal thickness (n= 3-5). **(D)** Epidermal permeability. Representative images of toluidine blue-treated ears (left) and quantification (right) (n= 3-5). **(A-D)** Bars represent average value and error bars depict standard deviation. *p<0.05, **p<0.01, ***p<0.001 using two-tailed unpaired Student's t-test.

We examined the effects of LC absence on UVR-induced keratinocyte EGFR activation. Epidermal EGFR showed increased phosphorylation by 1 hour after UVR exposure (Fig. 10A) [52], and we assessed this time point in subsequent experiments. Langerin-DTA mice had a modest reduction in homeostatic EGFR phosphorylation (Fig. 10B) and phosphorylation was not upregulated after UVR (Fig. 10C). These results suggested that LCs mediated the UVR-induced keratinocyte EGFR activation.

We then asked if the LC-dependent EGFR stimulation was protective. Treatment of Langerin-DTA mice with HB-EGF, a potent EGFR ligand [43], reduced UVR-induced apoptotic keratinocyte and monocyte accumulation (Fig. 11A,B). In vitro, adding human LCs and adding HB-EGF to keratinocytes had similar effects (Fig. 11C). Furthermore, siRNA-mediated knockdown of EGFR (Fig. 12A,B) or EGFR inhibition in keratinocytes (Fig. 12C,D) abolished the protective effect of LCs (Fig.12B,D) while EGFR inhibition in LCs did not (Fig. 12E,F). Together, these results suggested that LCs limit UVR-induced keratinocyte apoptosis and skin inflammation by stimulating keratinocyte EGFR

LC ADAM17 is critical for limiting photosensitivity and is activated by UVR

We asked whether LCs could be a key source of EGFR ligands. Both murine and human LCs expressed multiple EGFR ligands, and epigen and amphiregulin were upregulated by UVR exposure in murine LCs (Fig. 13A,B).

Figure 10

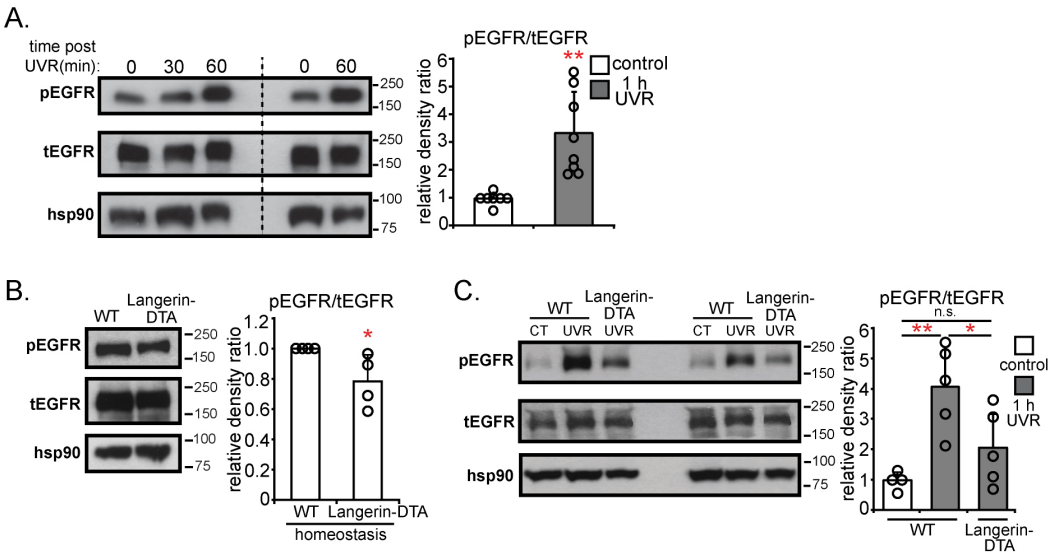

Figure 10. LCs are required for UVR-induced epidermal EGFR activation. Mice were exposed to UVR and ears were examined by Western blotting at the indicated time points after UVR exposure. **(A)** Timing of UVR-induced epidermal EGFR activation. WT mice were exposed to UVR and examined 30 minutes and 1 hour after UVR exposure. Left: Representative Western blot for phosphoEGFR (pEGFR), total EGFR (tEGFR), and hsp90 (loading control). Right: pEGFR:tEGFR relative density ratio (n= 7-8). **(B,C)** WT and Langerin-DTA mice were examined at homeostasis **(B)** or exposed to UVR and examined 1 hour after UVR **(C)** (n= 4-5). Left: Representative Western blots. Right: pEGFR:tEGFR relative density ratio. **(A-C)** Bars represent averages. Error bars depict standard deviation. *p< 0.05, **p< 0.01 using two-tailed unpaired Student's t-test.

Figure 11

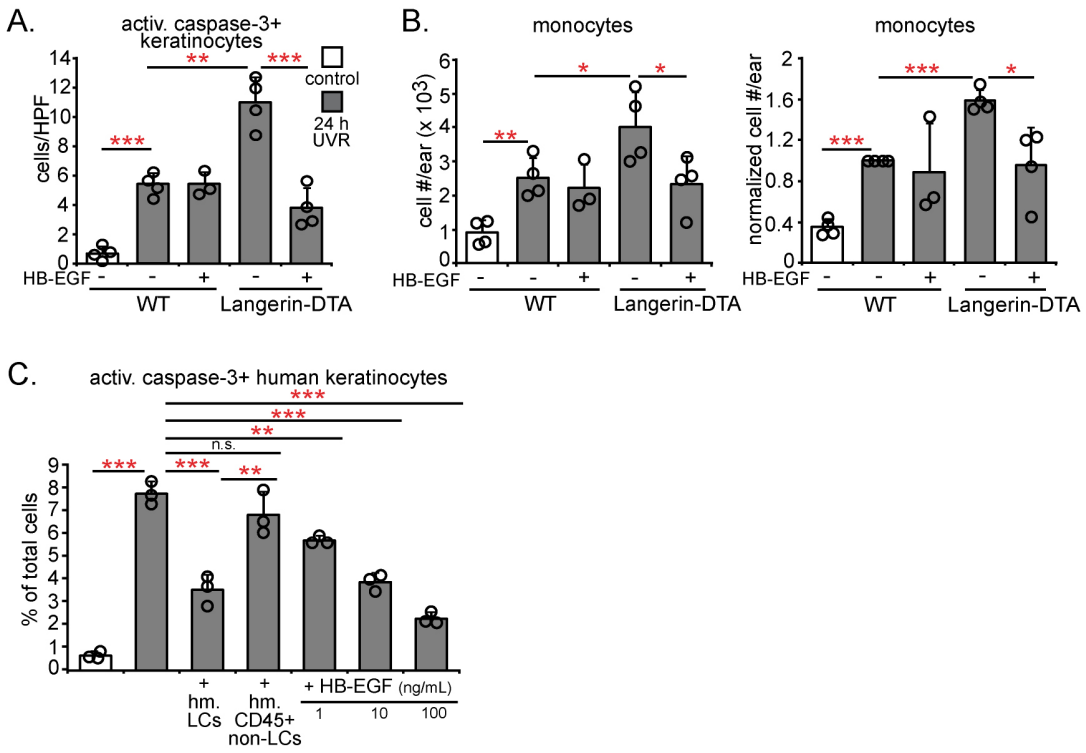

Figure 11. EGFR ligand supplementation rescues the Langerin-DTA phenotype and human LCs protect keratinocytes similar to EGFR ligands. (A,B) The ears of WT and Langerin-DTA mice were treated with vehicle or HB-EGF prior to UVR exposure (n= 3-4). **(A)** Activated caspase-3+ keratinocytes. **(B)** Absolute (left) and normalized (right) monocyte numbers. **(C)** Effect of human LCs on UVR-induced keratinocyte apoptosis. Primary human keratinocytes without or with indicated cells or recombinant HB-EGF were exposed to UVR and activated caspase-3+ keratinocytes were enumerated (n= 3 LC donors). **(A-C)** Bars represent averages. Error bars depict standard deviation. *p< 0.05, **p< 0.01, ***p< 0.001 using two-tailed unpaired Student's t-test.

Figure 12. LCs protect keratinocytes by stimulating keratinocyte EGFR. **(A)** Validation of siRNA-mediated EGFR knockdown in primary murine keratinocytes. Keratinocytes were treated with control or EGFR-targeted siRNAs (#1 and #2) and EGFR expression was measured 5 days later (on the day of UVR exposure as in Fig. 3F) by flow cytometry. Representative histogram of EGFR expression in keratinocytes. (n= 4). **(B)** Effect of keratinocyte EGFR knockdown on LC-mediated protection from UVR-induced keratinocyte apoptosis. Primary murine keratinocytes were treated with EGFR-targeted or control siRNAs before LC co-culture and UVR exposure. Activated caspase-3+ keratinocytes (n= 3 biological replicates). **(C)** Validation of pharmacological EGFR inhibition in primary murine keratinocytes. EGF-starved primary murine keratinocytes were pre-treated with vehicle or 2 μM PD168393 (an irreversible EGFR inhibitor) for 30 minutes, then treated with EGF (200 ng/mL) for 10 minutes, and phosphoEGFR was then measured by flow cytometry. Representative histogram of phosphoEGFR expression in keratinocytes (n= 3). **(D)** Effect of keratinocyte EGFR inhibition on LC-mediated protection from UVR-induced keratinocyte apoptosis. Primary murine keratinocytes were treated with vehicle or PD168393 before LC co-culture and UVR exposure. Activated caspase-3+ keratinocytes (n= 3 biologic replicates). **(E)** Validation of pharmacological EGFR inhibition in LCs. LCs were sorted from WT mice, serum-starved, pre-treated with vehicle, 2 μM PD168393, or an alternate EGFR inhibitor, CL-387,785 (1 μM) for 30 minutes, then treated with EGF (200 ng/mL) for 10 minutes, and phosphoEGFR measured by flow cytometry. Representative histogram of phosphoEGFR expression in LCs (n= 3). **(F)** Effect of LC EGFR inhibition on LC-mediated protection of keratinocyte s. Murine keratinocyte cultures without and with the indicated pre-treated LCs were exposed to UVR and activated caspase-3+ keratinocytes were enumerated (n= 3). **(B,D,F)** Bars represent averages. Error bars depict standard deviation. **p< 0.01, ***p< 0.001 using two-tailed unpaired Student's t-test.

Figure 12

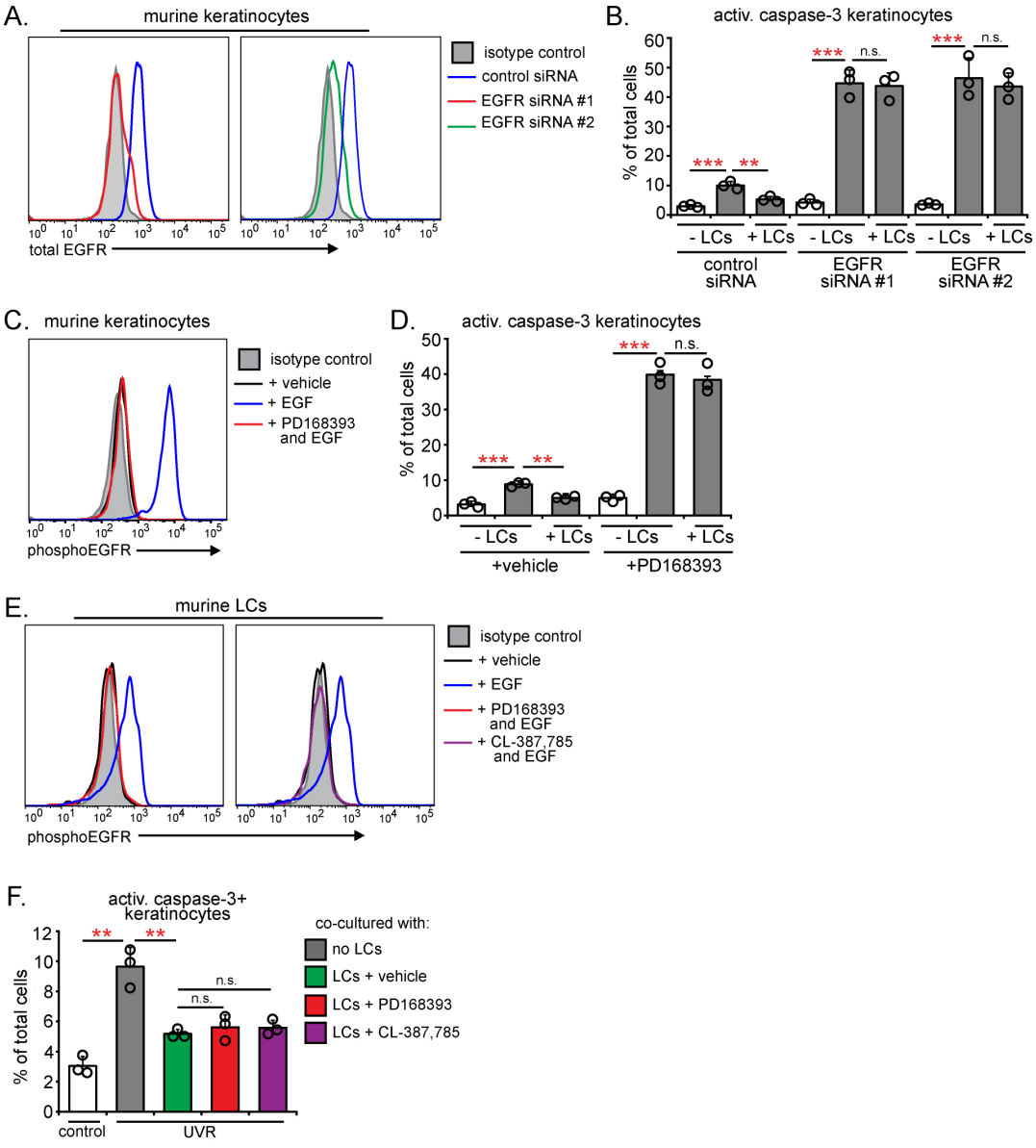
A.
murine keratinocytes
isotype control
control siRNA
EGFR siRNA #1
EGFR siRNA #2
total EGFR
B.
activ. caspase-3 keratinocytes
% of total cells
- LCs
+ LCs
control siRNA
EGFR siRNA #1
EGFR siRNA #2
C.
murine keratinocytes
isotype control
+ vehicle
+ EGF
+ PD168393 and EGF
phosphoEGFR
D.
activ. caspase-3 keratinocytes
% of total cells
+vehicle
+PD168393
E.
murine LCs
isotype control
+ vehicle
+ EGF
+ PD168393 and EGF
+ CL-387,785 and EGF
phosphoEGFR
F.
activ. caspase-3+ keratinocytes
co-cultured with:
no LCs
LCs + vehicle
LCs + PD168393
LCs + CL-387,785
% of total cells
control
UVR

A disintegrin and metalloprotease 17 (ADAM17) is a membrane-associated metalloprotease that is necessary for the cleavage and activation in cis of all EGFR ligands except EGF and β-cellulin [67], coincidentally, the 2 ligands not expressed or expressed at very low levels by LCs (Fig. 13A,B). Murine and human LCs expressed *Adam17* mRNA (Fig. 13C,D). The expression of both EGFR ligands and ADAM17 supported the idea that LCs were potentially capable of directly activating keratinocyte EGFR.

As LCs expressed multiple EGFR ligands, we assessed the role of LC-derived EGFR ligands by crossing ADAM17$^{flox/flox}$ mice [68] with Langerin-Cre$^{+/-}$ mice [69] to generate Langerin-Cre$^{+/-}$ADAM17$^{flox/flox}$ mice (LC-Ad17 mice) that have ADAM17 constitutively deleted from LCs (Fig. 14A). The Langerin-Cre driver itself had no effect on UVR-induced keratinocyte apoptosis (Fig. 14B), so experiments henceforth used Langerin-Cre$^{-/-}$ADAM17$^{flox/flox}$ mice as controls (WT). Although WT and LC-Ad17 mice had comparable LC numbers (Fig. 14C), LC-Ad17 mice showed reduced UVR-induced EGFR activation, similar to Langerin-DTA mice (Fig. 14D). LC-Ad17 mice also exhibited increased accumulation of apoptotic keratinocytes, monocytes, and monocyte-derived DCs (Fig. 14E-G), blunted epidermal hyperplasia (Fig. 4H), and increased epidermal permeability (Fig. 4I). Inducible deletion in LCs[70] of ADAM17 in Langerin-Cre-ER$^{+/-}$ ADAM17$^{flox/flox}$ mice also increased UVR-induced keratinocyte apoptosis and monocyte accumulation (Fig. 15A-E). HB-EGF treatment reduced the increased UVR-induced keratinocyte apoptosis and skin inflammation in the LC-Ad17 mice (Fig. 16A,B), supporting the idea that

Figure 13

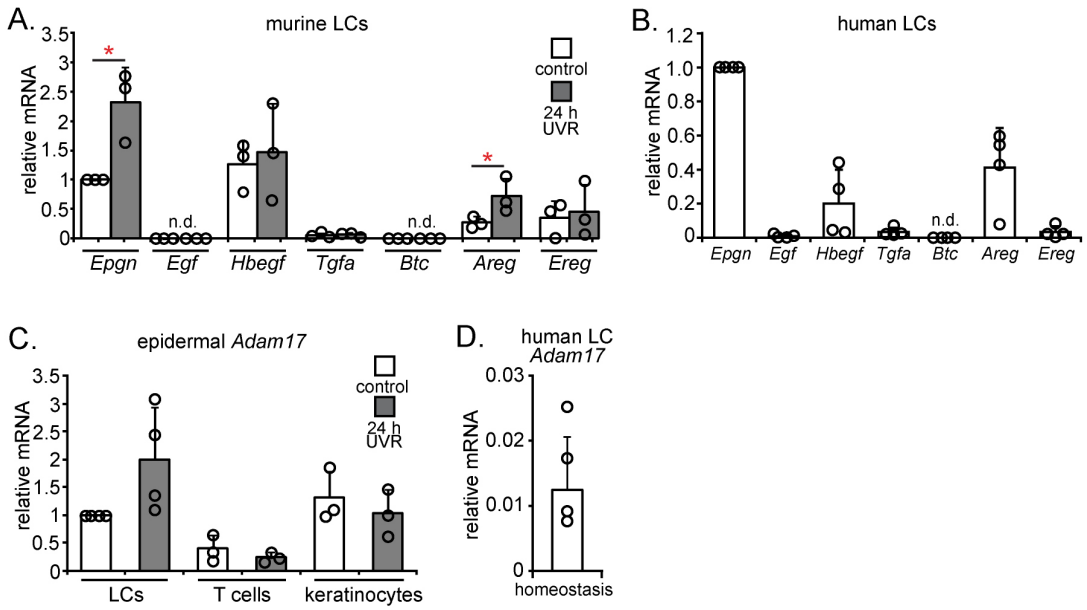

Figure 13. Murine and human LCs express EGFR ligands and *Adam17*. **(A)** LCs were sorted from WT mice exposed to UVR and from non-exposed WT control mice and examined. Murine LC EGFR ligand mRNA expression normalized to *Epgn* expression in WT control LCs (n=3). **(B)** LCs from healthy human skin were sorted and examined. Human LC EGFR ligand mRNA expression normalized to *Epgn* expression (n= 4 human LC donors). **(C)** LCs, T cells, and keratinocytes were sorted from WT mice exposed to UVR and from non-exposed WT control mice and examined. Murine epidermal cells *Adam17* mRNA expression normalized to *Adam17* expression in control LCs (n= 3-4). **(D)** Human LC *Adam17* mRNA expression relative to *Gapdh* expression (n= 4 human LC donors). **(A-D)** Bars represent averages. Error bars depict standard deviation. *p< 0.05 using two-tailed unpaired Student's t-test.

Figure 14. LC-derived ADAM17 is important for limiting UVR-induced keratinocyte apoptosis and skin injury. (A) *Adam17* expression in epidermal cell subsets sorted from WT and LC-Ad17 mice at homeostasis normalized to WT LC expression (n= 3). **(B)** Effect of Langerin-Cre driver on UVR-induced effects. Langerin-$Cre^{-/-}$ and Langerin-$Cre^{+/-}$ mice were exposed to UVR and activated caspase-3+ keratinocytes enumerated (n= 2-3). **(C-H)** WT and LC-Ad17 mice were treated with UVR and examined at the indicated time points after UVR exposure (n= 3-7). **(C)** LC numbers. **(D)** Epidermal EGFR phosphorylation. Left: Representative Western blot. Right: pEGFR:tEGFR ratio. Dashed lines are the values for the WT (blue) and Langerin-DTA (red) mice shown in the blot. **(E)** Activated caspase-3+ keratinocytes. **(F)** Absolute (left) and normalized (right) monocyte numbers. **(G)** Absolute (left) and normalized (right) monocyte-derived DC numbers. **(H)** Epidermal thickness. **(I)** Epidermal permeability. Left: Representative images. Right: Quantification. Bars represent averages **(A-G,I)** or median **(H)**. Error bars depict standard deviation **(A-G,I)** or interquartile range **(H)**. n.s.= not significant $p>0.05$, *$p<0.05$, **$p<0.01$, ***$p<0.001$ using two-tailed unpaired Student's t-test **(A-G,I)** or nonparametric non-directional Mann-Whitney *U* test **(H)**.

Figure 14

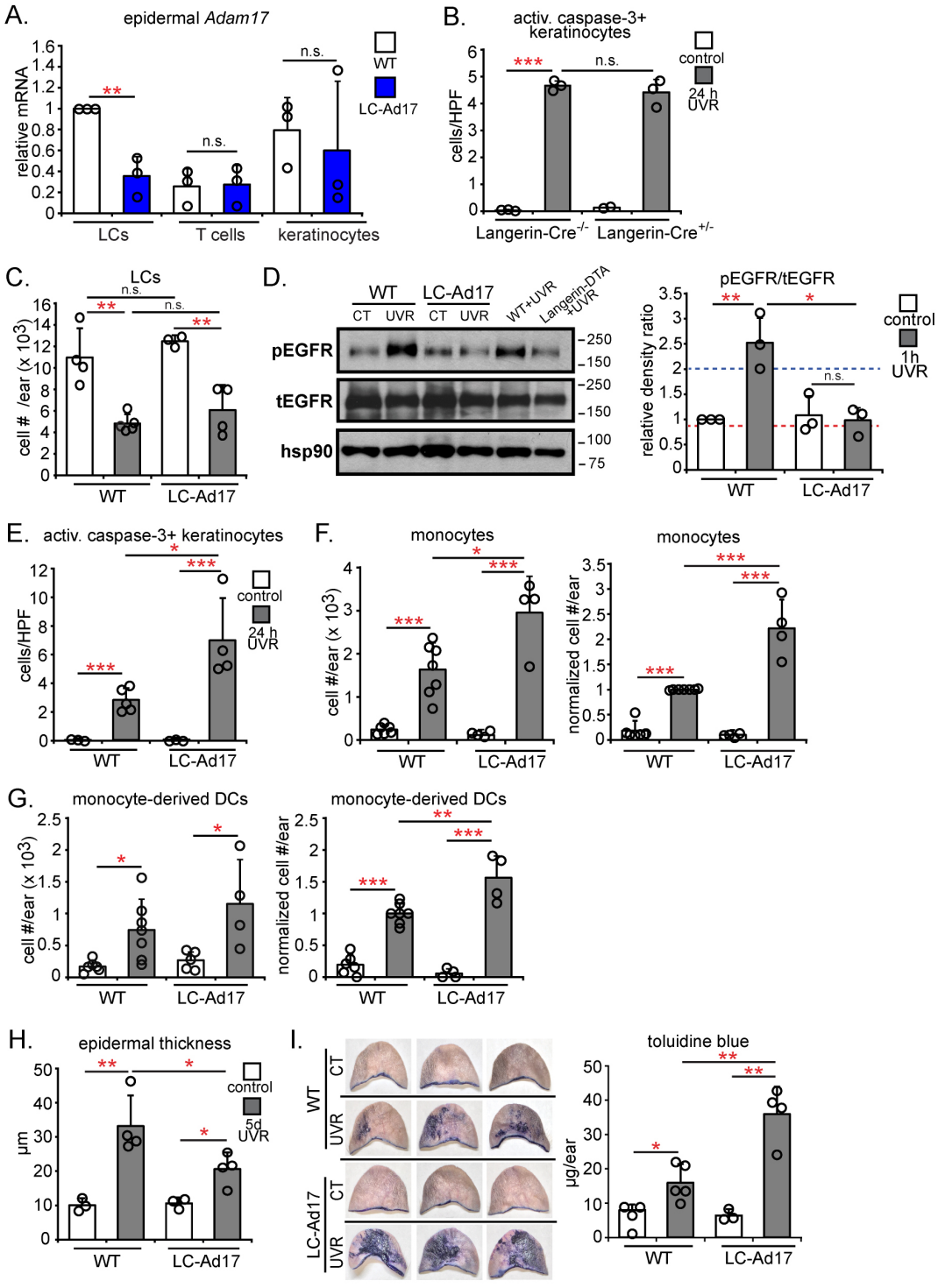
A.
epidermal Adam17
relative mRNA
WT
LC-Ad17
LCs
T cells
keratinocytes
n.s.
B.
activ. caspase-3+ keratinocytes
cells/HPF
control
24 h UVR
Langerin-Cre-/-
Langerin-Cre+/-
C.
LCs
cell # /ear (x 10^3)
WT
LC-Ad17
D.
WT
LC-Ad17
CT
UVR
WT+UVR
Langerin-DTA +UVR
pEGFR
tEGFR
hsp90
pEGFR/tEGFR
relative density ratio
control
1h UVR
E.
activ. caspase-3+ keratinocytes
F.
monocytes
cell #/ear (x 10^3)
normalized cell #/ear
G.
monocyte-derived DCs
H.
epidermal thickness
µm
control
5d UVR
I.
toluidine blue
µg/ear
CT
UVR

Figure 15

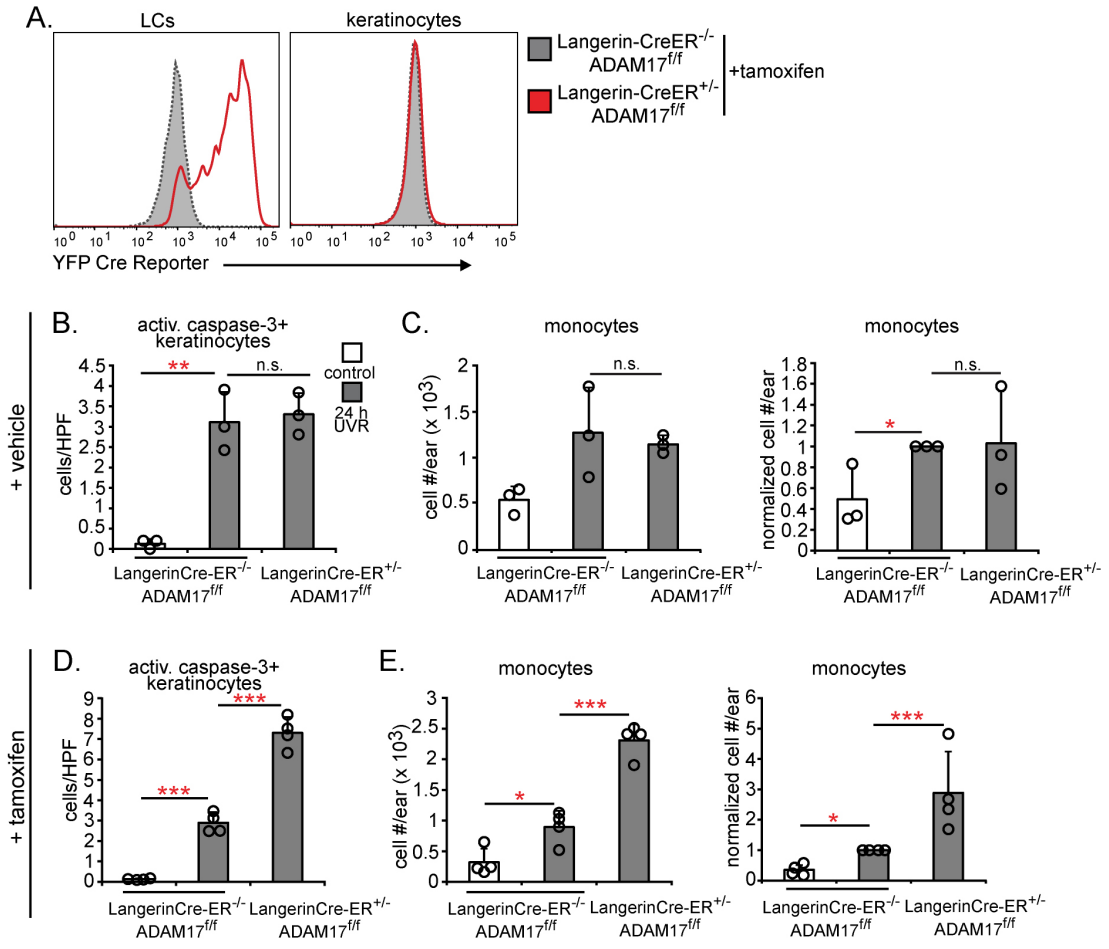

Figure 15. Inducible deletion of ADAM17 in LCs results in increased UVR-induced keratinocyte apoptosis and skin inflammation. (A-E) Langerin-Cre-ER$^{-/-}$ADAM17$^{flox/flox}$ and Langerin-Cre-ER$^{+/-}$ADAM17$^{flox/flox}$ mice containing a Rosa26.STOP^{fl}.YFP Cre reporter allele were generated and treated topically with vehicle (n= 3) **(B,C)** or 1 ng/mL 4-hydroxytamoxifen (n= 4) **(A,D,E)**. Six days later, they were either examined **(A)** or exposed to UVR and analyzed at 24 hours **(B-E).** **(A)** Cre expression in LCs. Shown is representative histogram of YFP levels in LCs and keratinocytes. **(B,D)** Activated caspase-3+ keratinocyte numbers. **(C,E)** Absolute (left) and normalized (right) monocyte numbers. **(B-E)** Bars represent average value and error bars depict standard deviation. n.s.= not significant p>0.05, *p<0.05, **p<0.01, ***p<0.001 using two-tailed unpaired Student's t-test.

Figure 16

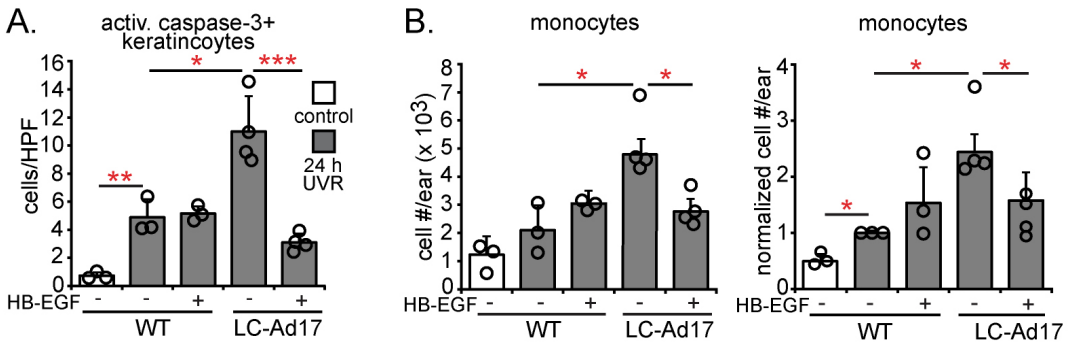

Figure 16. EGFR ligand supplementation rescues the phenotype of LC-Ad17 mice. (A,B) WT and LC-Ad17 mice were treated topically with vehicle or HB-EGF prior to UVR exposure and examined at 24 hours (n= 3-4). **(A)** Activated caspase-3+ keratinocytes. **(B)** Absolute (left) and normalized (right) monocyte numbers. **(A,B)** Bars represent average value and error bars depict standard deviation. *p<0.05, **p<0.01, ***p<0.001 using two-tailed unpaired Student's t-test.

the effect of LC ADAM17 deletion reflected an effect of EGFR signals. In vitro, ADAM17-deficient LCs were unable to protect keratinocytes from UVR-induced apoptosis (Fig. 17A), and ADAM17 blockade reduced the ability of human LCs to protect keratinocytes (Fig. 17B). These results suggested that LCs limit UVR effects via ADAM17 and stimulating keratinocyte EGFR.

The rapid LC-dependent increase in epidermal EGFR activation with UVR suggested that LC ADAM17 could be activated by UVR. Membrane-bound tumor necrosis factor receptor 1 (TNFR1) is a substrate for ADAM17 [67], and we quantified cell surface TNFR1 to measure ADAM17 activity. UVR can activate ADAM17 on keratinocytes [71] and UVR rapidly reduced TNFR1 levels on murine and human LCs in a ADAM17-dependent manner (Fig. 18A,B). These results suggested that ADAM17 on LCs can be rapidly activated by UVR.

To examine whether the UVR-induced ADAM17 activation actually resulted in EGFR ligand cleavage and release, we then collected conditioned supernatants from UVR-exposed LCs and assessed the ability of the supernatants to induce EGFR phosphorylation in EGFR-overexpressing A431 indicator cells (Fig. 19A,B). In contrast to supernatants from murine or human LCs that were not exposed to UVR, supernatants from UVR-exposed LCs induced a robust increase in A431 cell EGFR phosphorylation in an ADAM17-dependent manner (Fig. 19C,D). UVR exposure also caused murine keratinocytes to release more EGFR ligands, although this effect was less

Figure 17

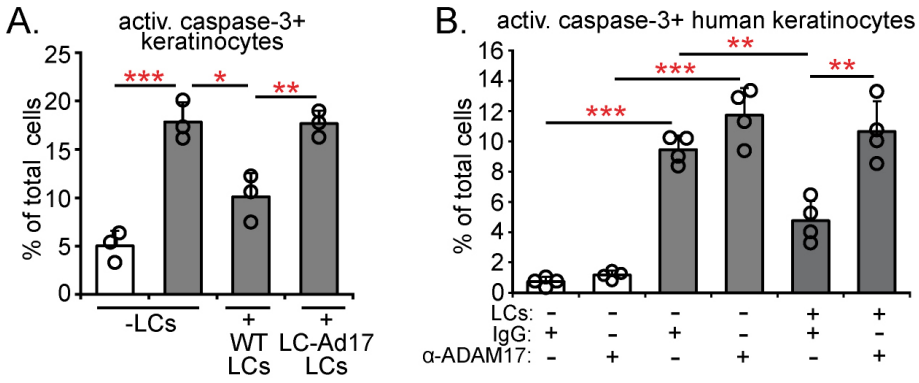

Figure 17. ADAM17 deficient LCs are unable to protect keratinocytes from UVR-induced apoptosis. (A) Murine keratinocytes without or with indicated LCs were exposed to UVR and activated caspase-3+ keratinocytes were enumerated (n= 3). **(B)** Human keratinocytes without or with LCs pretreated control-IgG or blocking anti-ADAM17-treated LCs were exposed to UVR and activated caspase-3+ keratinocytes were enumerated. **(A,B)** Bars represent averages. Error bars depict standard deviation. *p<0.05, **p<0.01, ***p<0.001 using two-tailed unpaired Student's t-test.

Figure 18

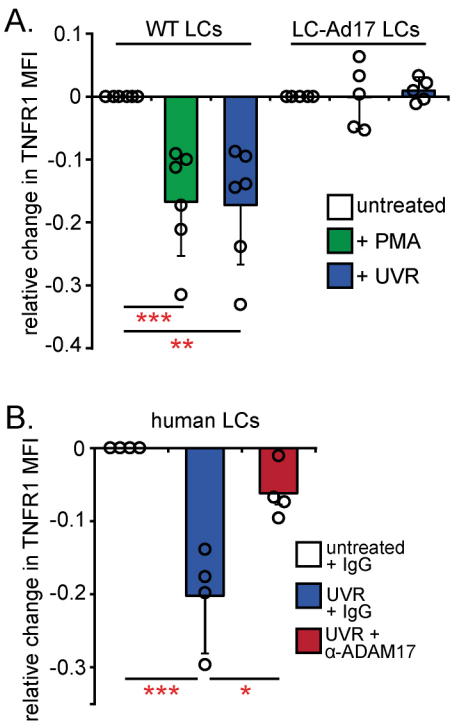

Figure 18. UVR directly activates LC ADAM17. Effect of UVR on ADAM17 activity in sorted murine **(A)** and human **(B)** LCs as measured by change in TNFR1 mean fluorescence intensity (MFI) upon indicated treatments (n= 5-6 mice; n=4 human donors). PMA is a known ADAM17 activator and response to PMA is a positive control [67]. LCs from LC-Ad17 mice are negative controls. **(A,B)** Bars represent averages. Error bars depict standard deviation. *p<0.05, **p<0.01, ***p<0.001 using two-tailed unpaired Student's t-test.

Figure 19. UVR directly induces LC derived EGFR ligand release. (A) Validation of EGFR ligand release assay using A431 cells. A431 indicator cells were serum-starved overnight then pre-treated for 15 minutes with vehicle, the irreversible EGFR inhibitors PD168393 (2 μM), or CL-387,785 (1 μM). The cells were then treated with EGF (100 ng/mL) for 10 minutes and phosphoEGFR was measured by flow cytometry (n= 2). **(B)** Schematic diagram of EGFR ligand release assay using A431 indicator cells. Cells (sorted murine LCs, sorted human LCs, or primary murine keratinocytes) were treated or not with UVR and the conditioned supernatant was collected and added to serum-starved A431 cells for 10 minutes. The A431 cells were then collected and phosphoEGFR was measured by flow cytometry as an indicator of the level of EGFR ligand in the conditioned supernatant. **(C,D)** Conditioned supernatants from untreated or UVR-exposed murine LCs in Fig. 19A **(C)** or human LCs in Fig. 19B **(D)** were added to A431 EGFR indicator cells and phosphoEGFR was measured 10 minutes later by flow cytometry. Left: Representative histogram. Right: Quantification relative to cells treated with control WT LC supernatants **(C)** or control IgG-treated LC supernatants **(D)**. **(E)** Characterization of murine primary keratinocyte EGFR ligand release. Confluent primary murine keratinocytes were exposed to UVR and the supernatant of these cells and non-exposed control keratinocytes was collected 45 minutes later and added to A431 cells as described in **B**. Left: Representative histogram of phosphoEGFR expression in the A431 cells. Right: Quantification of A431 cell phosphoEGFR expression normalized to the expression with control keratinocyte supernatants. *$p<0.05$, **$p<0.01$, ***$p<0.001$ using two-tailed unpaired Student's t-test.

Figure 19

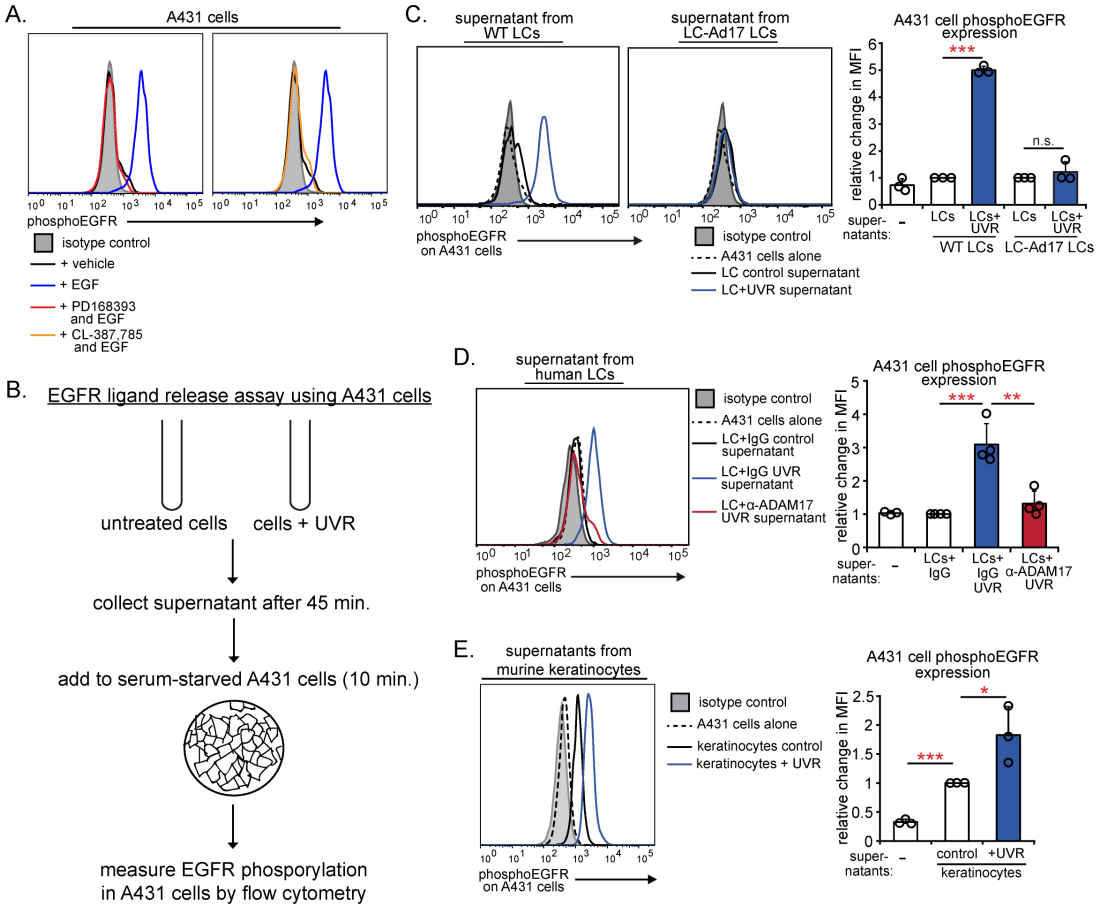
A.
A431 cells
phosphoEGFR
isotype control
+ vehicle
+ EGF
+ PD168393 and EGF
+ CL-387,785 and EGF
B.
EGFR ligand release assay using A431 cells
untreated cells
cells + UVR
collect supernatant after 45 min.
add to serum-starved A431 cells (10 min.)
measure EGFR phosporylation in A431 cells by flow cytometry
C.
supernatant from WT LCs
supernatant from LC-Ad17 LCs
phosphoEGFR on A431 cells
isotype control
A431 cells alone
LC control supernatant
LC+UVR supernatant
A431 cell phosphoEGFR expression
relative change in MFI
***
n.s.
super-natants:
–
LCs
LCs+ UVR
LCs
LCs+ UVR
WT LCs
LC-Ad17 LCs
D.
supernatant from human LCs
phosphoEGFR on A431 cells
isotype control
A431 cells alone
LC+IgG control supernatant
LC+IgG UVR supernatant
LC+α-ADAM17 UVR supernatant
A431 cell phosphoEGFR expression
relative change in MFI
***
**
super-natants:
–
LCs+ IgG
LCs+ IgG UVR
LCs+ α-ADAM17 UVR
E.
supernatants from murine keratinocytes
phosphoEGFR on A431 cells
isotype control
A431 cells alone
keratinocytes control
keratinocytes + UVR
A431 cell phosphoEGFR expression
relative change in MFI
***
*
super-natants:
–
control
+UVR
keratinocytes

robust than that seen in the LCs (Fig. 19E). These data further established that UVR can trigger ADAM17 activation on LCs and showed that this activation can result in greater availability of active EGFR ligand. Together, our results suggested that there is an LC-keratinocyte axis whereby UVR induces LC ADAM17 activation and consequent EGFR ligand cleavage, leading to increased keratinocyte EGFR activation, which limits UVR-induced keratinocyte apoptosis and skin injury.

Chapter III: CHARACTERIZATION OF A DYSFUNCTIONAL LC-KERATINOCYTE AXIS IN PHOTOSENSITIVITY

Photosensitivity in LE is often due to UVR exposure and since we have delineated a protective LC-keratinocyte axis, we asked whether photosensitivity in lupus mouse models could in part reflect dysfunction of this LC-keratinocyte axis. We also asked whether there were signs of a dysfunctional LC-keratinocyte axis in human SLE. Better understanding of photosensitivity in LE is needed to implement better treatment strategies for skin manifestations and to potentially prevent systemic flares of SLE.

The LC-keratinocyte axis is dysfunctional in photosensitive SLE models

MRL-*Fas*^{lpr} mice are SLE model mice that are known to be photosensitive, developing cutaneous lesions similar to human LE lesions with multiple days of UVR treatment[72-74]. We asked whether MRL-*Fas*^{lpr} mice were more photosensitive than control mice at 24 hours after a single dose of UVR treatment. We used non-photosensitive Balb/c and MRL-MpJ mouse strains as control mice [74]. We examined MRL-*Fas*^{lpr} mice at 8 weeks of age, an age when these mice show early autoimmunity but no significant renal disease and no spontaneous skin lesions. As previously shown, UVR exposure induces increased apoptotic keratinocyte accumulation in MRL-*Fas*^{lpr} mice (Fig. 20A)[75], along with skin plasma cell accumulation (Fig. 20B). Consistent with the

Figure 20. MRL-Faslpr mice have a dysfunctional LC-keratinocyte axis. **(A-E)** MRL-*Fas*^{lpr} and non-lupus control (Balb/c and/or MRL-MpJ) mice were exposed to UVR and examined as indicated. **(A)** Activated caspase-3+ keratinocytes (n= 2-4). **(B)** MRL-*Fas*^{lpr} and non-lupus MRL-MpJ or Balb/c mice were exposed to UVR for 6 consecutive days and skin from these and non-exposed control mice were examined 24 hours after the final exposure. Skin plasma cells with 6 days of UVR exposure (n= 4). **(C)** Epidermal EGFR phosphorylation at 1 hour after UVR exposure. Left: Representative Western blot. Right: pEGFR:tEGFR ratio. **(D,E)** LCs were sorted from control and UVR exposed Balb/c and MRL-Faslpr mice 24 hours after UVR and examined (n= 4). **(D)** LC EGFR ligand mRNA expression normalized to Balb/c control LCs. **(E)** LC *Adam17* mRNA expression normalized to control Balb/c LCs. **(A-E)** Bars represent averages. Error bars depict standard deviation. n.s= not significant $p>0.05$, *$p<0.05$, **$p<0.01$, ***$p<0.001$ using two-tailed unpaired Student's t-test.

Figure 20

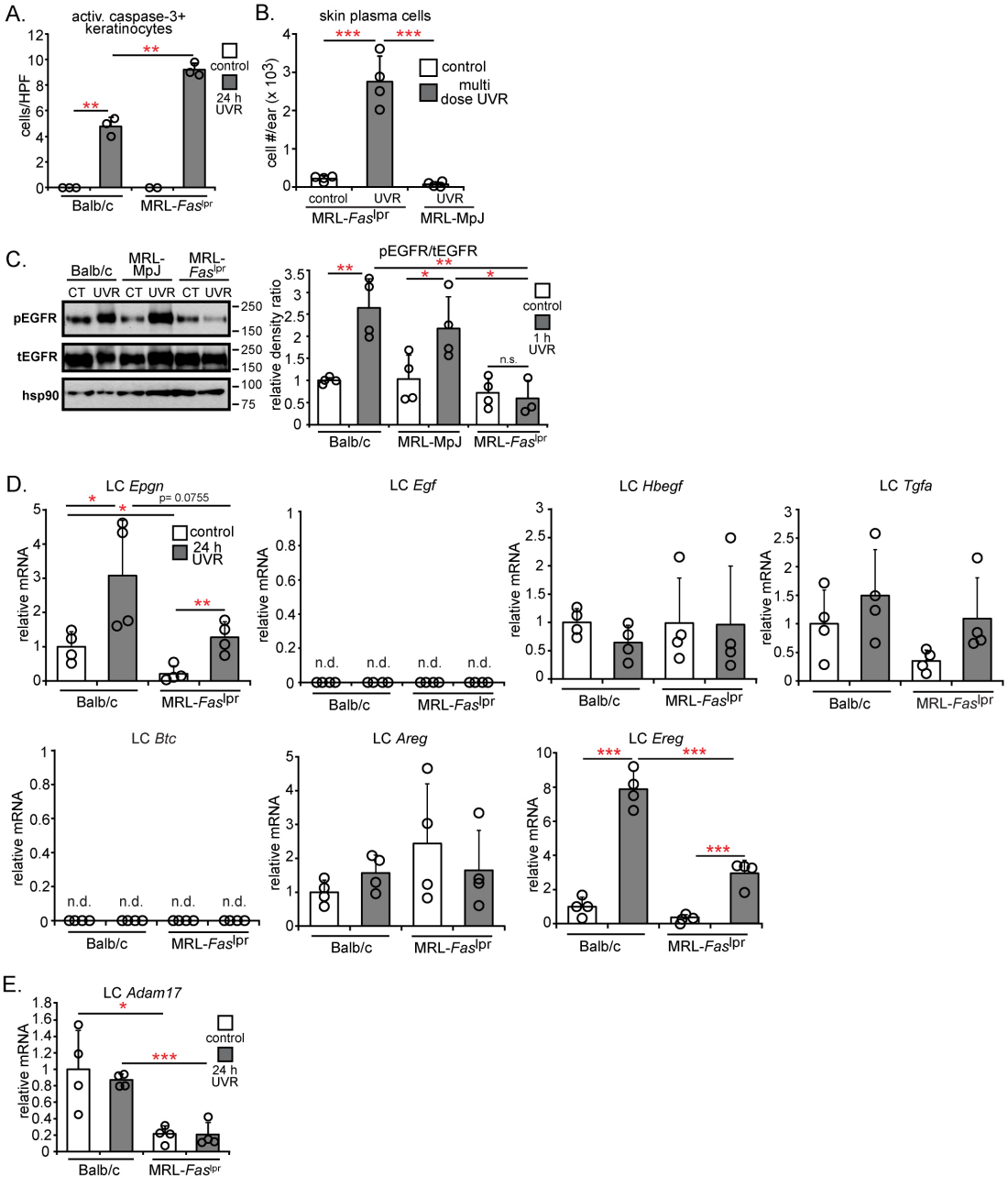
A.
activ. caspase-3+ keratinocytes
cells/HPF
control
24 h UVR
Balb/c
MRL-Faslpr
B.
skin plasma cells
cell #/ear (x 10³)
control
multi dose UVR
control
UVR
UVR
MRL-Faslpr
MRL-MpJ
C.
Balb/c
MRL-MpJ
MRL-Faslpr
CT UVR CT UVR CT UVR
pEGFR
tEGFR
hsp90
pEGFR/tEGFR
relative density ratio
control
1 h UVR
n.s.
Balb/c
MRL-MpJ
MRL-Faslpr
D.
LC Epgn
p= 0.0755
control
24 h UVR
relative mRNA
LC Egf
n.d.
LC Hbegf
LC Tgfa
LC Btc
LC Areg
LC Ereg
E.
LC Adam17
control
24 h UVR

possibility of a dysfunctional LC-keratinocyte axis, MRL-*Fas*^{lpr} mice showed reduced UVR-induced epidermal EGFR phosphorylation (Fig. 20C).

LC numbers are comparable between MRL-*Fas*^{lpr} mice and Balb/c controls [76] and we asked about their ability to protect skin. MRL-*Fas*^{lpr} LCs showed a trend toward reduced expression of epigen, the most abundantly expressed EGFR ligand, with UVR, and reduced expression of epiregulin, a ligand expressed at relatively low levels (Fig. 20D, Fig. 13A). *Adam17* mRNA, on the other hand, was reduced in MRL-*Fas*^{lpr} mice by about 70% at homeostasis and after UVR exposure (Fig. 20E). Consistent with the reduced ADAM17 expression, MRL-*Fas*^{lpr} LCs showed no UVR-induced ADAM17 activation as indicated by TNFR1 changes or release of EGFR ligands (Fig. 21A,B). In vitro, MRL-*Fas*^{lpr} LCs did not limit UVR-induced keratinocyte apoptosis (Fig. 21C) while WT LCs could limit UVR-induced apoptosis of MRL-*Fas*^{lpr} keratinocytes (Fig. 21C), suggesting that LC dysfunction was the critical defect that led to the increased UVR sensitivity in MRL-*Fas*^{lpr} mice. These data together suggested that MRL-*Fas*^{lpr} LCs, because of reduced ADAM17 and potentially because of reduced EGFR ligand expression, were unable stimulate epidermal EGFR, thus contributing to photosensitivity.

We also examined the B6.Sle1yaa model of SLE. These mice carry the Sle1 lupus susceptibility locus derived from lupus-prone NZB2410 mice along with the Y chromosome autoimmune accelerator locus whose activity is attributable to TLR7 duplication [77-79]. The mice develop lymphadenopathy by 3 months (Fig. 22A), splenomegaly and autoantibody production by 4 months,

Figure 21

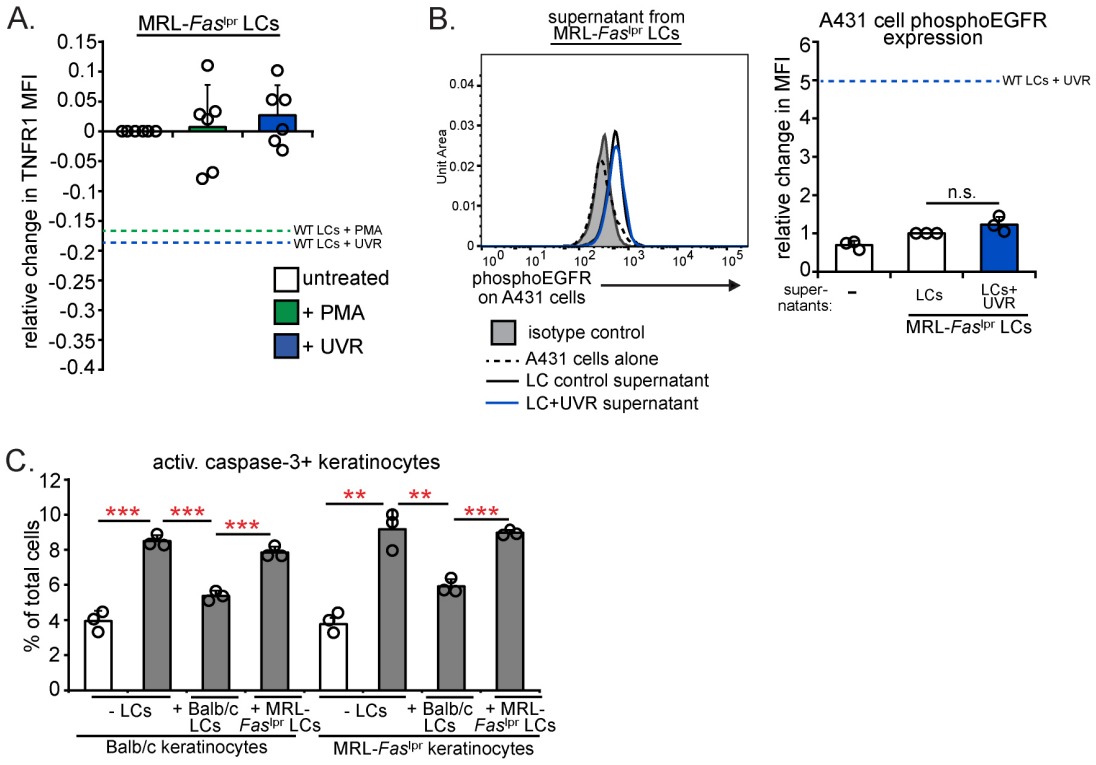

Figure 21. MRL-*Fas*^{lpr} LCs show no UVR-induced ADAM17 activation and EGFR ligand release and are unable to limit UVR-induced keratinocyte apoptosis. (A) MRL-*Fas*^{lpr} LC ADAM17 activity. LCs sorted from MRL-*Fas*^{lpr} mice were treated with PMA or UVR and the percent change in TNFR1 MFI relative to that of untreated LCs was measured 45 minutes later by flow cytometry (n= 6). Dashed lines indicate the relative change in TNFR1 MFI observed in WT mice treated with PMA (green) or UVR (blue) as in Fig. 18A. **(B)** Conditioned supernatants from untreated and UVR-exposed MRL-*Fas*^{lpr} LCs were added to A431 EGFR indicator cells and phosphoEGFR in the A431 cells was measured 10 minutes later by flow cytometry (n=3). Dashed line indicates the relative change in phosphoEGFR MFI observed with UVR-exposed WT LC supernatants as in Fig. 19C. **(C)** Effect of MRL-*Fas*^{lpr} LCs on keratinocyte apoptosis. Balb/c or MRL-*Fas*^{lpr} keratinocytes were exposed to UVR without or with indicated LCs and activated caspase-3+ keratinocytes were enumerated (n= 3). **(A,B)** Each symbol represents 1 mouse. **(C)** Each symbol represents a biological replicate, which is the average of 1-4 replicate wells. **(A-C)** Bars represent average value and error bars depict standard deviation. n.s.= not significant $p>0.05$, *$p<0.05$, **$p<0.01$, ***$p<0.001$ using two-tailed unpaired Student's t-test.

Figure 22. B6.Sle1Yaa mice are photosensitive. (A) Popliteal lymph node cellularity at 3 months of age (n= 7). **(B)** Activated caspase-3+ keratinocyte numbers in 6 week old B6.Sle1Yaa mice or age-matched B6 mice (n= 2-3). **(C)** Activated caspase-3+ keratinocyte numbers in 8-12 month old B6.Sle1Yaa mice or age-matched B6 mice (n= 3). **(D,E)** 8-12 month old B6.Sle1Yaa mice and age-matched B6 mice were exposed to UVR for 6 days starting at day 0 (d0) and ears harvested 24 hours after the final exposure (n= 3). **(D)** Images of representative ears at the indicated time points of UVR exposure. White arrows indicate visible lesions. **(E)** Normalized number of plasma cells in the skin as measured by flow cytometry. **(A-C,E)** Bars represent average value; error bars depict standard deviation. n.s.= not significant $p>0.05$, *$p<0.05$, ***$p<0.001$ using two-tailed unpaired Student's t-test.

Figure 22

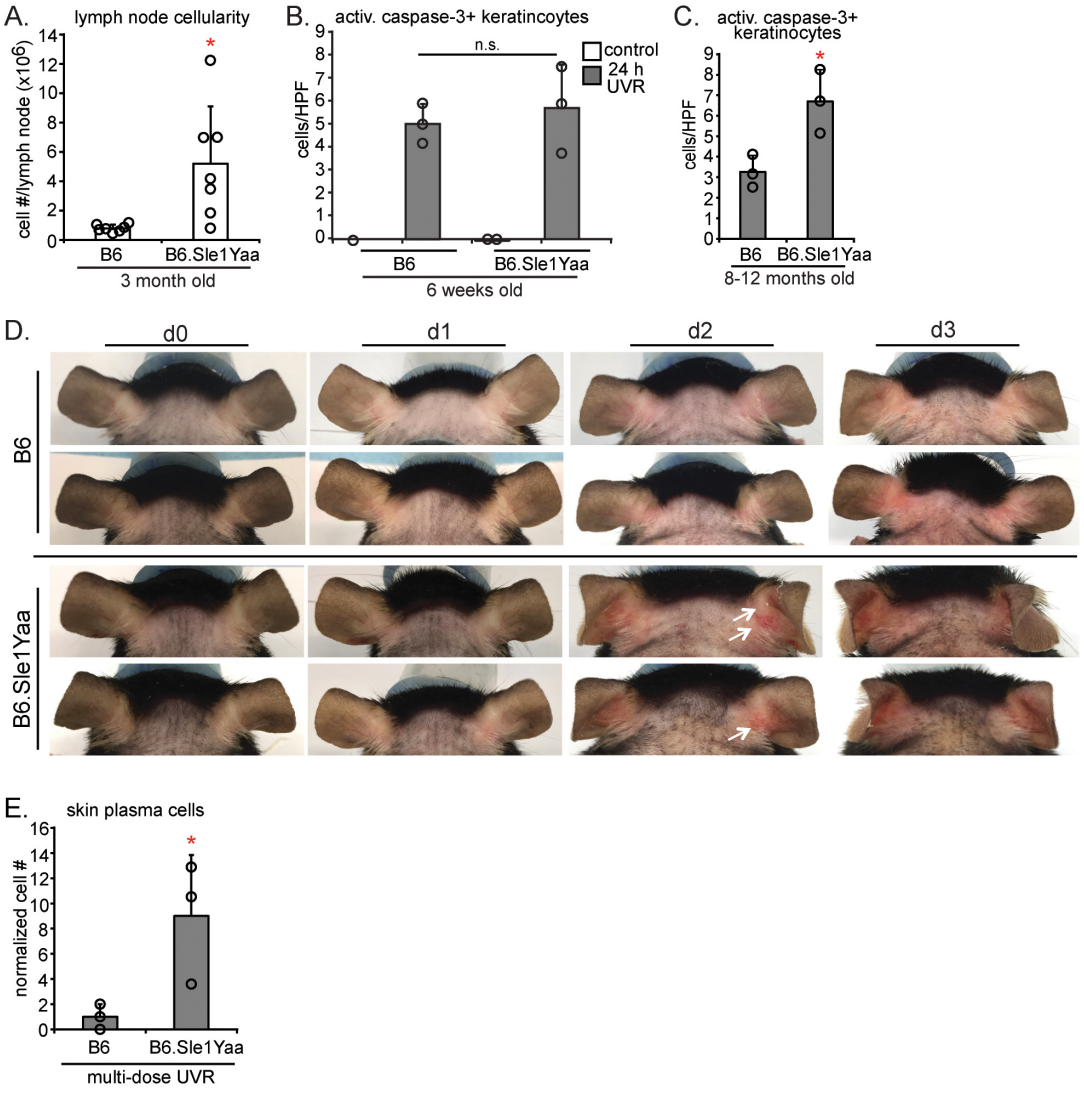
A.
lymph node cellularity
cell #/lymph node (x10^6)
B6
B6.Sle1Yaa
3 month old
B.
activ. caspase-3+ keratincoytes
n.s.
control
24 h UVR
cells/HPF
B6
B6.Sle1Yaa
6 weeks old
C.
activ. caspase-3+ keratinocytes
cells/HPF
B6
B6.Sle1Yaa
8-12 months old
D.
d0
d1
d2
d3
B6
B6.Sle1Yaa
E.
skin plasma cells
normalized cell #
B6
B6.Sle1Yaa
multi-dose UVR

and nephritis by 12 months [77]. However, this model has not been shown to be photosensitive. Six week old B6.Sle1yaa mice did not show increased UVR-induced keratinocyte apoptosis (Fig. 22B), but 8-12 month old B6.Sle1yaa mice did (Fig. 22C). Upon multi-day UVR treatment, 8-12 month old B6.Sle1yaa mice developed skin lesions as early as 2 days while B6 mice did not (Fig. 22D). The skin findings were associated with the presence of plasma cells in the skin (Fig. 22E). These results indicated that diseased B6.Sle1yaa mice are photosensitive.

The 8-12 month old B6.Sle1yaa mice also showed reduced UVR-induced epidermal EGFR activation relative to controls (Fig. 23A). LC numbers were unchanged and only the EGFR ligand amphiregulin was reduced (Fig. 23B,C), but B6.Sle1yaa LCs showed reduced *Adam17* mRNA expression (Fig. 23D), similar to MRL-*Fas*^{lpr} mice. These data together suggested that photosensitivity in both SLE models may be attributable at least in part to a dysfunctional LC-keratinocyte axis whereby LCs are less able to produce activated EGFR ligands to stimulate keratinocyte EGFR.

A dysfunctional LC-keratinocyte axis in human SLE

We examined human SLE skin for signs of a dysfunctional LC-keratinocyte axis. Non-sun-exposed, nonlesional SLE skin [80] showed decreased LC numbers relative to healthy control skin (Fig. 24A), suggesting an abnormality in LC function and a potential for reduced input of EGFR ligands. Epidermal EGFR phosphorylation was also reduced in SLE skin

Figure 23. A dysfunctional LC-keratinocyte axis exists in B6.Sle1Yaa mice. (A) 8-12 month old B6.Sle1Yaa mice and age-matched B6 control mice were exposed to UVR and examined at 1 hour after UVR exposure. Epidermal EGFR phosphorylation (n= 3). Left: Representative Western blot. Right: pEGFR:tEGFR ratio. **(B-D)** 8-12 month old B6.Sle1yaa mice or age-matched B6 mice were examined at homeostasis. **(B)** Percent of LCs in skin as measured by flow cytometry (n= 4). **(C,D)** B6.Sle1yaa LC expression of EGFR ligands and *Adam17*. LCs were sorted from homeostatic B6 and B6.Sle1yaa mice and mRNA expression was normalized to that of B6 mice (n= 5). n.d.= not detectable. **(A-D)** Each symbol represents 1 mouse**.** Bars represent average value; error bars depict standard deviation. n.s.= not significant $p>0.05$, *$p<0.05$, ***$p<0.001$ using two-tailed unpaired Student's t-test.

Figure 23

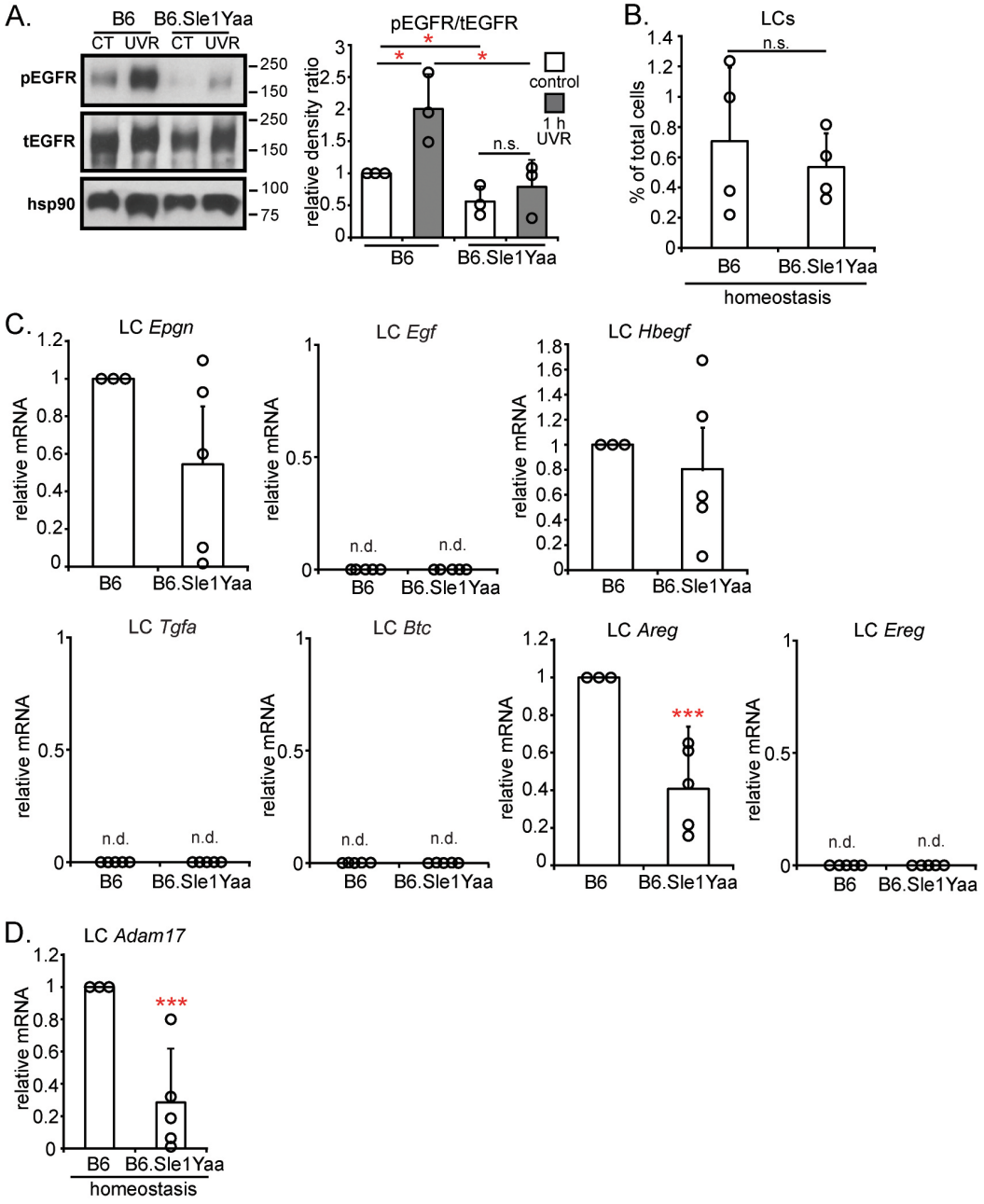
A.
B6
B6.Sle1Yaa
CT UVR CT UVR
pEGFR
tEGFR
hsp90
250
150
250
150
100
75
pEGFR/tEGFR
relative density ratio
control
1 h UVR
n.s.
B6
B6.Sle1Yaa
B.
LCs
n.s.
% of total cells
B6
B6.Sle1Yaa
homeostasis
C.
LC Epgn
LC Egf
LC Hbegf
LC Tgfa
LC Btc
LC Areg
LC Ereg
relative mRNA
n.d.
***
D.
LC Adam17
relative mRNA
***
B6
B6.Sle1Yaa
homeostasis

Figure 24

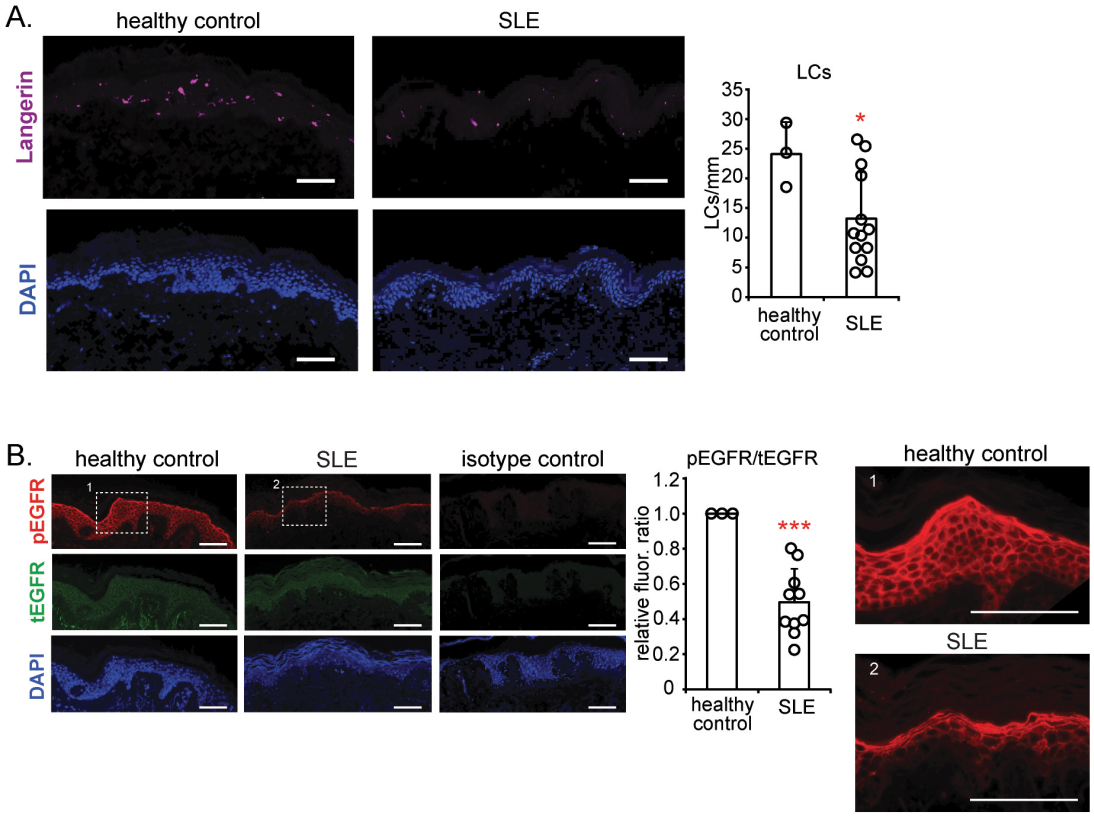

Figure 24. A dysfunctional LC-keratinocyte axis exists in human SLE. **(A,B)** LC numbers and epidermal EGFR phosphorylation in human SLE skin (n= 3 healthy controls, 10-13 SLE patients). **(A)** Left: Representative images of anti-Langerin (purple) and DAPI (blue) staining. Right: LC numbers per mm of tissue. **(B)** Left: Representative images of anti-pEGFR (red), anti-tEGFR (green), and DAPI (blue) staining. Middle: Relative pEGFR:tEGFR fluorescence intensity normalized to healthy control skin. Right: Magnified insets from pEGFR stain. **(A,B)** Bars represent averages. Error bars depict standard deviation. n.s= not significant $p>0.05$, *$p<0.05$, **$p<0.01$, ***$p<0.001$ using two-tailed unpaired Student's t-test.

(Fig. 24B). These data support the idea that the LC-keratinocyte axis is dysfunctional in human SLE.

Topical EGFR ligand reduces photosensitivity in an SLE model

We asked whether EGFR ligand supplementation could reduce photosensitivity in MRL-*Fas*^{lpr} mice. Multi-day UVR exposure has been shown to increase complement and immunoglobulin deposition in skin [75] and we observed that this regimen also led to ulcerations with a neutrophil-dominant infiltrate (Fig. 25A-E). In contrast, MRL-MpJ mice remained grossly unaffected (Fig. 25B). Topical treatment with HB-EGF (Fig. 25A) reduced the severity of UVR-induced skin lesions (Fig. 25B-E) and monocyte accumulation (Fig. 25F). HB-EGF also reduced germinal center B cells (Fig. 26A) and plasma cells (Fig. 26B) in skin-draining lymph nodes, suggesting that modulating skin function EGFR signaling may impact systemic immunity. These findings suggest that compensating for a dysfunctional LC-keratinocyte axis by providing EGFR ligand can be used as an approach to treating photosensitivity.

Figure 25. Topical EGFR ligand reduces photosensitivity in MRL-*Fas*^{lpr} mice. (A) Experimental scheme for MRL-*Fas*^{lpr} or MRL-MpJ non-lupus control mice in **(B-E)** (n= 4). Mouse ears and back skin were topically treated with HB-EGF for 2 days before and on the first day of UVR exposure and examined 24 hours after the final exposure. **(B)** Representative images of ears. **(C)** Representative images of back skin; boxes outline lesional areas. Magnified images of back skin on the right. **(D)** Representative H&E images of ear skin. Neutrophil-dominant infiltrate (dashed box); ulceration (*). **(E)** Ear histopathology score. **(F)** Absolute monocyte numbers. **(E,F)** Bars represent averages. Error bars depict standard deviation. *****$p<0.05$, ***$p<0.001$ using two-tailed unpaired Student's t-test.

Figure 25

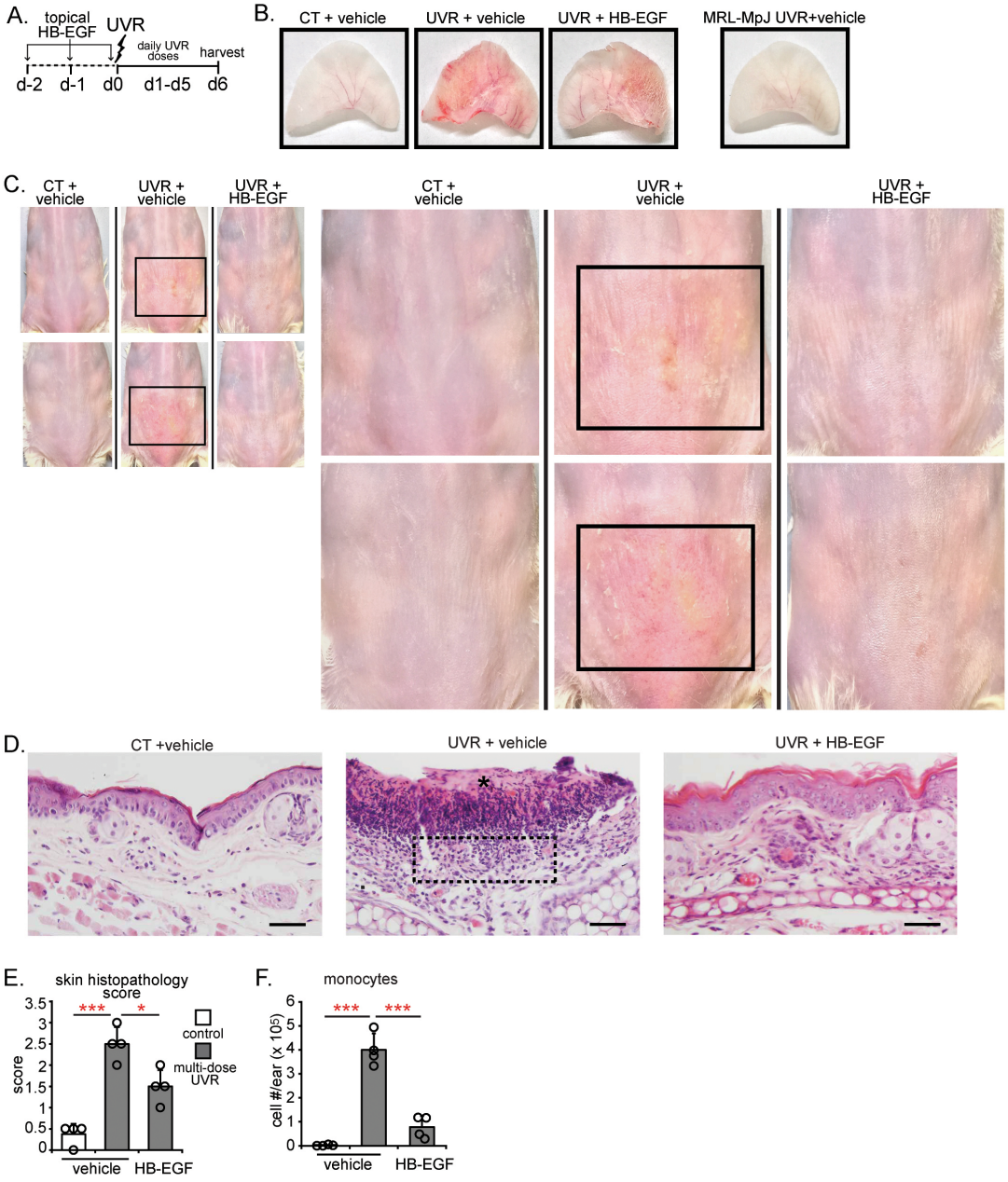
A.
topical HB-EGF
UVR
daily UVR doses
harvest
d-2
d-1
d0
d1-d5
d6
B.
CT + vehicle
UVR + vehicle
UVR + HB-EGF
MRL-MpJ UVR+vehicle
C.
CT + vehicle
UVR + vehicle
UVR + HB-EGF
CT + vehicle
UVR + vehicle
UVR + HB-EGF
D.
CT +vehicle
UVR + vehicle
UVR + HB-EGF
E.
skin histopathology score
score
control
multi-dose UVR
vehicle
HB-EGF
F.
monocytes
cell #/ear (x 10^5)
vehicle
HB-EGF

Figure 26

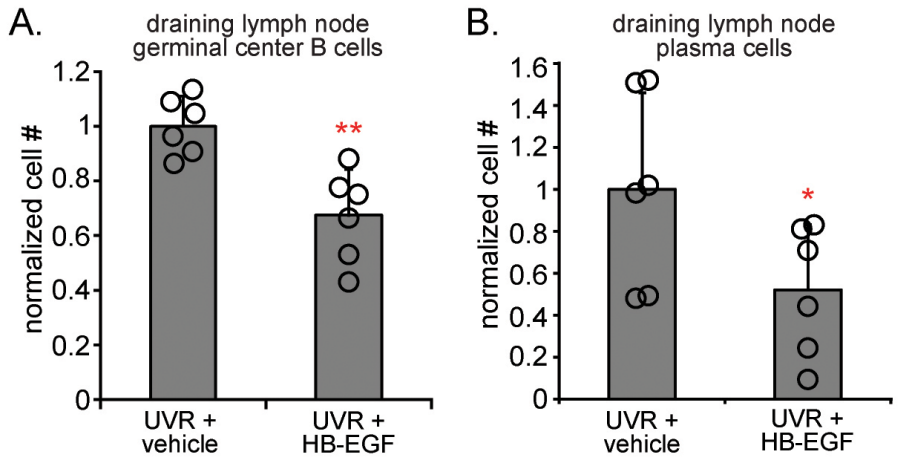

Figure 26. Topical EGFR ligand reduces draining lymph node B cell responses in MRL-*Fas*^{lpr} mice. (A,B) Normalized number of germinal center B cells **(A)** and plasma cells **(B)** in skin draining lymph nodes (auricular and inguinal). **(A,B)** Each symbol represents either inguinal or auricular lymph nodes from multiple mice. Error bars depict standard deviation. *p<0.05 and **p<0.01 using two-tailed unpaired Student's t-test.

CHAPTER IV: DISCUSSION AND PERSPECTIVES

LCs are best known as antigen-presenting cells, and the findings here establish LCs as direct modulators of keratinocyte function and skin integrity whereby LCs limit sensitivity to UVR-induced keratinocyte apoptosis and skin injury. Murine and human LCs express EGFR ligands and ADAM17. ADAM17 in LCs is critical for limiting UVR-induced effects and we show that UVR directly activates murine and human LC ADAM17 and leads to the provision of activated, soluble EGFR ligands to stimulate keratinocyte EGFR. We show that keratinocyte EGFR expression is critical for LC-mediated protection and that murine and human LCs can directly protect keratinocytes from UVR-induced apoptosis in an ADAM-17 dependent manner. LC abnormalities may contribute to dysfunction of the LC-keratinocyte axis in SLE, leading to photosensitivity and we show that two different SLE mouse models, MRL-*Fas*^{lpr} and B6.Sle1Yaa mice, have reduced LC ADAM17 expression and/or function and reduced epidermal UVR-induced EGFR activation, suggesting that there is a dysfunctional LC-keratinocyte axis in these models. In addition, non-sun-exposed, nonlesional human SLE skin had reduced LC numbers and reduced epidermal EGFR phosphorylation, suggesting that human SLE skin may also have a dysfunctional LC-keratinocyte axis. EGFR ligand supplementation may be an approach to treating photosensitivity, as this treatment resulted in reduced severity of photosensitive lesions in SLE model mice (Fig. 27).

Figure 27

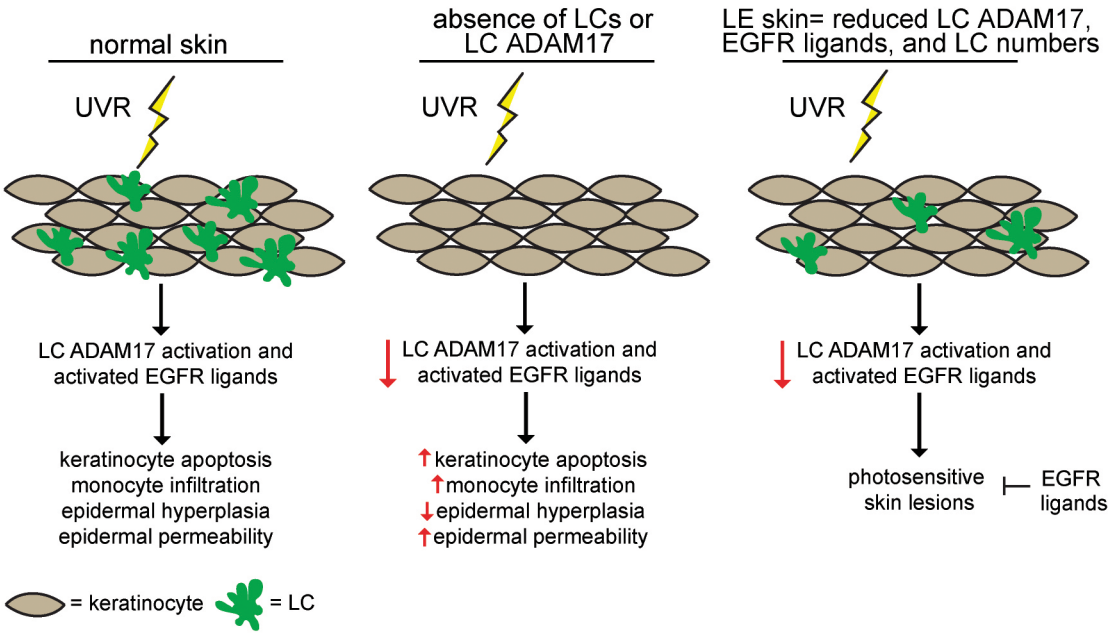

Figure 27. Model of protective LC-keratinocyte axis and dysfunction of this axis in LE photosensitivity. In normal skin, LCs express ADAM17 and EGFR ligands. UVR stimulates LC ADAM17 activity and LCs provide activated EGFR ligands and limit the extent of keratinocyte apoptosis and skin injury. In the absence of LCs or with ADAM17 deletion in LCs, UVR-induced keratinocyte apoptosis and skin injury are increased. In LE, LCs are less able to provide activated EGFR ligands to keratinocytes, because of reduced ADAM17, reduced EGFR ligand expression, and/or reduced LCs, leading to photosensitivity. The provision of EGFR ligands could be a useful therapeutic approach for photosensitivity.

The LC-keratinocyte axis appears to be a stress survival mechanism. During homeostasis, keratinocyte ADAM17 plays a major role in maintaining skin integrity and barrier function [53], and our results indicating that LCs have only a modest role in maintaining epidermal EGFR phosphorylation during homeostasis is consistent with this. In contrast, LCs and LC ADAM17 had an important role in limiting skin injury with UVR, suggesting a scenario in which, in times of stress, keratinocytes require an extra source of EGFR ligands and LCs function as this source. That LC ADAM17 responded more robustly to UVR than keratinocyte ADAM17 further supported a role for LCs in providing a critical source of EGFR ligands in the setting of stress. It is still unclear whether keratinocytes are the major source of EGFR ligands at homeostasis, but it will be interesting in future studies to determine if this is true and if this role switches during times of stress, such as UVR exposure, and LCs then become the major source of EGFR ligands. This role in promoting survival during stress is similar to the role of DCs that we have delineated in inflamed lymph nodes and fibrotic skin [54,55]. Murine LCs are closely related to macrophages in ontogeny but have classical DC functions [35] and our findings suggest that LCs behave as DCs in maintaining epidermal integrity in times of stress.

The findings in this study identify a novel function for LCs- being a direct modulator of keratinocyte health. This idea of myeloid cells regulating stromal cells in the skin has been explored by other groups and has garnered significant attention in the past few years. Recently, our group has shown that

during skin fibrosis, DCs can directly regulate adipose-derived stromal cell (ADSC) survival leading to modulation of skin fibrosis[54]. Previously, Gwendolyn Randolph and colleagues showed that CCR7 and IRF4-dependent DCs regulate lymphatic vessel permeability and fibrosis in adipose tissue near the skin surface[56], providing another example of how myeloid cells can regulate stromal cells in the skin and surrounding areas. It will be interesting to see what other stromal cells in the skin are regulated by myeloid cells and how these putative interactions are potentially dysregulated in disease.

Our study reveals the complexity of mechanisms for protecting barrier surfaces. Regulatory T cells and group 2 innate lymphoid cells have recently been shown to be critical sources of the EGFR ligand amphiregulin in protecting lung and colonic epithelium, respectively, during inflammatory processes[81,82]. In these models, upregulated amphiregulin expression was induced by alarmins from the injured tissues. In contrast, LCs had a tonic albeit modest influence on epidermal EGFR phosphorylation and LCs appeared to be “immediate responders” via ADAM17 activation within minutes directly by the injury-inducing stimulus. Whether injured keratinocyte signals contribute to inducing the upregulation of epigen and amphiregulin by LCs that we observed at 24 hours and whether LCs are unique among immune cells in direct activation of ADAM17 remains to be seen, but our study with the other studies together suggest that there are distinct immediate versus early layers of regulation to protect barrier surfaces.

During the preparation of this manuscript, Hatakeyama et al [83] suggested that LCs help to resolve UVR-induced skin inflammation at day 5 and later after UVR exposure by ingesting and clearing apoptotic keratinocytes. We show distinct findings, focusing on immediate events after UVR exposure. Furthermore, we detected essentially no activated caspase-3+ Langerin+ cells at 24 hours after exposure in WT mice and in LC-keratinocyte co-cultures, suggesting that LC phagocytosis of apoptosis keratinocytes was minimal both in situ and in our co-cultures. Thus, while we do not rule out a role for LCs in clearing apoptotic keratinocytes at later time points, our study firmly establishes a role for LCs in limiting keratinocyte apoptosis early on. Furthermore, that pharmacologic EGFR inhibition and ADAM17 deletion in LCs showed the same defects in epidermal hyperplasia and barrier function as Langerin-DTA mice supports the idea that these later functional deficits are related to the early effects on keratinocytes.

Based on the data in this study, it is possible that LCs limit UVR-induced keratinocyte apoptosis, which in turn limits keratinocyte expression of various chemokines and cytokines that promote inflammation, such as monocyte recruitment to the skin. The specific chemokines and cytokines that UVR-induced apoptotic keratinocytes may produce and whether this production leads to downstream inflammatory effects is still unknown. Our study suggested that LCs limit monocyte recruitment to the UVR-exposed skin and raised the possibility that accumulated monocytes contribute to the increased epidermal permeability. Interestingly, UVR has long been noted to

deplete LCs from the skin, and this depletion correlated with myeloid cell accumulation [84]. Our results would suggest that the UVR-mediated depletion of LCs from the skin caused the myeloid cell accumulation and that stronger or chronic UVR exposure would further deplete LCs, leading to even greater myeloid cell accumulation. EGFR activity has been shown to limit keratinocyte CCL2 expression [29], but the extent to which LCs alter chemokine expression by keratinocytes, fibroblasts, or endothelial cells needs to be examined more directly in future studies. Elkon and colleagues [85] recently showed that monocytes may be a major source of type I interferon a few days after UVR exposure, and it would be interesting to understand whether type I interferon contributed to the increased epidermal permeability. As UVR is also associated with immune suppression in healthy humans but increased autoimmunity in SLE patients [19,84], it will be interesting to understand whether the monocyte and monocyte-derived cells participate in differentially modulating immunity after UVR exposure in healthy and LE patients.

Our study is relevant for understanding photosensitivity in human disease in several ways. First, we showed that the LC-keratinocyte axis is dysfunctional in two SLE models and the reduced EGFR phosphorylation in human SLE skin suggested that this axis may also be dysfunctional and contribute to photosensitivity in human SLE. LC numbers were reduced in human SLE skin, and whether the reduced epidermal EGFR phosphorylation reflected the LC reduction, other defects such as reduced LC ADAM17 or EGFR ligand expression, remains to be determined. While LC-independent

keratinocyte-intrinsic dysfunction may also lead to reduced epidermal EGFR phosphorylation and will need to be considered, the reduced LC numbers suggest failure of LC development or survival or perhaps increased migration to draining lymph nodes and suggest that LCs may be dysfunctional in human SLE. Second, our data showed that the protective effects of LCs reflected protective effects to UVA and possibly also UVB; given that sunlight is comprised primarily of UVA [86], our data are relevant for better understanding the mechanisms that protect against the effects of sunlight exposure in LE patients. Further understanding of LC function and regulation in SLE will be interesting, as will understanding whether there are similar defects in photosensitivity associated with other disorders [21].

The fact that LCs are reduced in number and epidermal EGFR phosphorylation is reduced in human SLE skin raises the question as to why signs of a dysfunctional LC-keratinocyte axis would be present at homeostasis in non UVR-exposed skin. This raises the possibility that human SLE skin is primed or predisposed to be more inflamed after sunlight exposure due to this abnormal state at homeostasis. Since LCs are already reduced and baseline epidermal EGFR phosphorylation is already reduced, then perhaps any activation with UVR is insufficient to protect the skin or perhaps no activation will occur at all. In future studies, it will be interesting to see if LC ADAM17 expression and/or function is reduced in human SLE and whether this is a contributing factor to reduced epidermal EGFR phosphorylation. It would also be interesting to explore whether sun-exposed skin or lesional skin in human

SLE patients have reduced LC ADAM17 or reduced epidermal EGFR phosphorylation relative to non-sun-exposed or nonlesional skin.

The limitations of the study are: 1) we do not yet know if human SLE LCs are less able to provide activated EGFR ligands or protect keratinocytes from UVR, 2) we do not yet understand how UVR activated ADAM17, 3) we do not yet understand how LCs are dysregulated in the SLE models, and 4) we do not yet understand whether there is LC-keratinocyte dysfunction in photosensitivity in other conditions.

Our data suggest that topical EGFR stimulation could be a treatment to prevent the development of photosensitive cutaneous lesions in LE. While the potential for carcinogenesis should be considered [87], topical EGF is being investigated for rashes associated with the use of EGFR inhibitors to treat lung cancer patients who are most likely immune compromised [88] (clinicaltrials.gov; trials NCT03051880 and NCT03047863). Furthermore, in mouse models of colitis-associated cancer, EGFR inhibited tumor development, likely by improving epidermal function and reducing inflammation [89]. This study provides preliminary findings that could be used to develop a novel therapeutic for LE patients. The findings are truly translational because it raises the idea that LE patients can utilize a topical EGFR ligand to either prevent or treat photosensitive lesions. More work is needed to further solidify this translational application, but these findings are promising.

We observed a reduction in draining lymph node germinal center cells and plasma cells (both of which are systemic features of SLE [90,91]) with HB-

EGF topical treatment, suggesting that EGFR stimulation may also improve the systemic aspects of photosensitivity in SLE. It is unknown whether topically applied HB-EGF traveled to the draining lymph node and acted directly or whether modulating the state of the skin led to decreased systemic disease. Since sun-exposure can lead to exacerbation or flares in systemic disease [22,23], delineating a mechanism whereby treating the skin can reduce systemic effects of the disease could lead to novel methods to treat or prevent SLE flares. The potential ability to reduce systemic disease by topically treating the skin also raises the exciting possibility of treating systemic disease via the skin, a less invasive and more patient-friendly method. More work is needed to further explore these ideas but the prospects for clinical applications are exciting to consider.

Our findings suggest that EGFR-stimulating agents should be investigated for photosensitivity in LE and potentially other autoimmune and dermatologic conditions. The LC-keratinocyte axis that we have delineated in this study may be applicable in a variety of skin disorders so it will be interesting to see if this axis exists in other disorders and if correcting this axis can also be used to treat these other illnesses. We propose that EGFR ligands or other EGFR-stimulating agents may be a novel therapeutic approach for photosensitivity in LE and should also be explored for other skin disorders.

Future studies related to this dissertation project include: 1) further characterization of human SLE LCs, 2) determining what regulates ADAM17 in

LCs and how this is abnormal in LE, and 3) exploring whether LCs regulate other stromal cells in the skin.

We show that LCs are reduced in number in human SLE skin, but future studies will attempt to measure *Adam17* mRNA expression in human SLE LCs, potentially by using readily available single cell RNA-sequencing data [92]. Whether or not *Adam17* is reduced in human SLE LCs, it will still be interesting in future studies to see if isolated LCs from human SLE skin are able to protect keratinocytes from UVR-induced apoptosis as efficiently as LCs from healthy control skin. Other factors about human SLE LCs may be abnormal as well, such as cell shape, cell motility, activation marker expression, and survival, and these will all be interesting to examine in future studies as well.

We also show that LC ADAM17 is activated with UVR exposure and that *Adam17* mRNA expression is reduced in SLE model mice, but the specific factors or mechanisms that modulate LC ADAM17 activity or expression are still unclear. It has been shown that iRhoms control ADAM17 maturation and activation [46,93,94], but it is still unknown if UVR modulates iRhom activity. It has also been suggested that UVR-induced reactive oxygen species (ROS) can modulate ADAM17 activity [71], but whether or not ROS production plays a role in LC ADAM17 activity and whether ROS production is abnormal in LCs from SLE model mice still needs further examination. Molecules such as type I interferons, that are present at abnormal levels in LE patients and SLE model

mice [85,95-101], may also play a regulatory role in LC ADAM17 activity and experiments to address this will be conducted in future studies.

Our data delineates a novel function for LCs as regulators of keratinocyte survival and it will be interesting in future studies to ask whether LCs regulate other stromal cells in the skin. Since LCs travel from the epidermis to the dermis as they migrate to the lymph node, it is possible that LCs can interact with fibroblasts, blood vessels, and lymphatic vessels in the dermis. Future studies will examine the state of these dermal stromal cells in Langerin-DTA mice and explore putative mechanisms by which LCs may regulate these stromal cells as well.

CHAPTER V: MATERIALS AND METHODS

Study design

Controlled experiments were designed using mouse models, in vitro systems, and human skin. For all mouse experiments, animals were randomly assigned to experimental groups. Sample sizes were determined based on previously published experiments using similar tissues and assays [54,55]. No data was excluded, each experiment was performed with at least 3 biological replicates, and all data were reliably reproduced. Investigators were not blinded to group allocation during experiments and data acquisition. During data analysis, investigators were not blinded for flow cytometry, Western blot, epidermal permeability, and mRNA experiments but were blinded for histology/immunofluorescence and lesion measurements. Sample numbers and numbers of replicates for independent experiments are included in each figure legend. Each symbol in the figures represents 1 mouse, human, or biological replicate (the average of replicate wells in in vitro experiments). All primary data are included in Table S3.

Mice

Mice from 6-12 weeks old were used unless otherwise stated and were sex and aged-matched. Both male and female mice were used for experiments, except for B6.Sle1yaa mice, in which only males were used because the model is dependent in part on the autoimmune accelerator locus on the Y

chromosome [77]. C57BL/6J, Langerin-DTA, Rag1$^{-/-}$, Balb/c, MRL-MpJ, MRL-*Fas*^{lpr}, and B6.Sle1yaa mice were originally from Jackson Laboratory (JAX) and bred at our facility. CCR2-GFP and CCR2-DTR mice [62] were bred at our facility. Rag1$^{-/-}$ mice were intercrossed with Langerin-DTA mice to generate Rag1$^{-/-}$ Langerin-DTA mice. ADAM17$^{flox/flox}$ mice [68] were intercrossed with Langerin-Cre$^{+/-}$ mice [69,70] (National Cancer Institute (NCI)), and Langerin-Cre$^{ER+/-}$YFP mice [70] to generate LC-Ad17 and Langerin-Cre$^{ER+/-}$ADAM17$^{flox/flox}$ mice, respectively. All animal procedures were performed in accordance with the regulations of the Institutional Animal Use and Care Committee at the Hospital for Special Surgery and Weill Cornell Medicine.

UVR treatments

In vivo: Four FS40T12 sunlamps that emit UVA and UVB at a 40:60 ratio [59] were used as the UVR source. We determined 1000 J/m^2 UVR to be the minimal dose that caused visible dilation in the ears of C57BL/6J mice at 24 hours and used this dose for all experiments unless otherwise indicated. For multi-dose experiments with Langerin-DTA mice, mice were shaved 24 hours before the first UVR exposure. SLE model mice were shaved 24 hours before the first UVR exposure and then exposed to 500 J/m^2 of UVR for 6 consecutive days for lesion development experiments.

In vitro: Mouse and human primary keratinocytes and LCs were exposed to 500 J/m^2 UVR with the same UVR lamps as above.

Mouse treatments

For indicated 24 hour experiments, HB-EGF (2ug; R&D Systems) dissolved in dimethyl sulfoxide (DMSO) was applied to each ear 15 minutes prior to UVR exposure. For long-term lesion development experiments, mice were shaved in a small area on the lower back. At 24 hours, HB-EGF was applied on the ears as above and on the shaved back area (8ug) for three consecutive days. Mice received their first dose of UVR on the last day of HB-EGF treatment.

Flow cytometric staining and sorting

For staining of murine whole skin, single cell suspensions of skin were generated as previously described [54]. Briefly, ear skin was excised, finely minced, digested in collagenase type II (616 U/mL; Worthington Biochemical Corporation), dispase (2.42 U/mL; Life Technologies), and DNAse1 (80 μg/mL; Sigma-Aldrich), incubated at 37°C while shaking at 100 rpm, triturated with glass pipettes, and filtered. For murine epidermal cell staining or sorting, ear and trunk skin was incubated in dispase at 37°C for 45 minutes. The epidermis was then scraped off and finely minced before digestion in collagenase type II.

For flow cytometry analysis, the following gating strategies were used after excluding debris and non-single cells: *LCs:* Lineage-, CD45+ CD11b+ CD24+, CD11c+, MHCII+; *monocytes*: Lineage- (CD3, B220, NK, Ly6G)-, CD45+, CD11b+, CD24-, Ly6C+, MHCII-; *monocyte-derived DCs*: Lineage- CD45+

CD11b+ CD24- Ly6C^{hi-lo}, MHCII+; *CD11b+ DCs*: Lineage- CD45+ CD24- CD11b+ Ly6C- CD64- CD11c+ MHCII+; *CD11b- DCs*: Lineage- CD45+ CD11b- CD24+ CD11c+ MHCII+; *macrophages:* Lineage- CD45+ CD11b+ CD24- CD64+; *neutrophils:* Lineage+ CD11b+ Ly6C^{med}, side scatter (SSC)^{hi}; *T cells*: epidermal CD45+, CD11b-, CD3+; *keratinocytes*: epidermal CD45-, CD31-, EpCAM+ or total skin CD45-, CD31-, CD49f+, Sca1+, EpCAM+; *skin plasma cells*: CD45+, B220^{lo}, CD3-, intracellular IgG^{hi}; *lymph node germinal center B cells*: CD3-, B220+, PNA+; *lymph node plasma cells:* CD3-, B220^{lo}, CD138+. LCs, monocytes, monocyte-derived DCs, CD11b+ DCs, CD11b- DCs, and macrophages were gated according to Tamoutounour et al. [61]. Primary and secondary antibodies are described in Table S1 and Table S2.

For flow cytometry analysis, cells were analyzed using a FACSCanto (BD Biosciences) and FlowJo Software (Tree Star). Cells were sorted using a BD Influx.

To measure phosphoEGFR by flow cytometry, cells were serum- or EGF-starved, pretreated with 2 mM $NaVO_3$ for 15 minutes, fixed with 4% paraformaldehyde for 15 minutes at room temperature, and then permeabilized with ice-cold methanol (90%) for 30 minutes on ice. The cells were then stained with anti-phosphoEGFR Tyr1068 (Cell Signaling) followed by anti-rabbit Alexa647 (Jackson Immunoresearch).

For human LC and CD45+ non-LC isolations, fresh skin samples were obtained from patients undergoing elective reconstructive surgery. Skin samples were cut into small pieces and incubated for 30 min at 37°C and 5%

CO_2 in prewarmed DMEM/F-12 (Stem Cell Technologies) with dispase II (1 IU/ml; Roche Diagnostics) to facilitate separation of the epidermis from the dermis. The epidermis was gently peeled away from the dermis and placed in RPMI 1640 supplemented with 10 mM HEPES, 1% penicillin/streptomycin (Media Lab, MSKCC), 50 mM L-glutamine (Cellgro), 50 μM β-mercaptoethanol (Gibco, Life Technologies), and 10% heat-inactivated pooled healthy human serum (Atlanta Biologicals). The epidermal sheets were then finely minced and digested with collagenase as described for mouse epidermis. LCs (CD45+ CD1a+ HLADR+) and non-LC CD45+ cells (CD45+ CD1a- HLADR-) were sorted. Sorted cells had a purity ≥ 95%.

Histology, immunofluorescence staining, and quantifications

For immunofluorescence staining of murine skin, frozen unfixed mouse skin was sectioned, fixed with cold acetone for 10 minutes, and stained as indicated [55]. Epidermal activated caspase-3+ cells per high powered field (40x magnification) were quantified by a blinded observer using ImageJ (NIH) software and classified as activated caspase-3+ keratinocytes (Langerin- and CD3-), LCs (Langerin+), or T cells (CD3+).

Formalin-fixed paraffin embedded murine skin was stained with hematoxylin and eosin, and epidermal thickness was measured by a blinded observer using ImageJ software (NIH).

For immunofluorescence staining of cell culture experiments, polystyrene chamberslides (Lab-Tek) with cultured keratinocytes were washed with PBS,

fixed with 4% paraformaldehyde for 20 minutes, permeabilized and blocked with Triton-X (0.2%) and BSA (1%), and stained as indicated. Activated caspase-3+ and total DAPI+ cells were quantified with ImageJ software by a blinded observer and the percent of activated caspase-3+ Langerin- cells (keratinocytes) and activated caspase-3+ Langerin+ cells (LCs) was calculated.

For immunofluorescence staining of human skin, formalin-fixed paraffin-embedded tissue sections were rehydrated and underwent antigen retrieval at 60°C in 10 mM citrate buffer, pH 6.0 for 20 hours followed by enzymatic retrieval with Carezyme III: Pronase Kit (Biocare Medical) for 15 minutes. Sections were then stained as indicated. The fluorescence intensity of phosphoEGFR and total EGFR was measured using ImageJ software and the fluorescence intensity of the isotype control was subtracted. The ratio of phosphoEGFR:total EGFR was then calculated and normalized to the ratio for the healthy control samples that were stained at the same time as the SLE samples. Langerin+ cells in the epidermis were counted by a blinded observer using ImageJ software and normalized to the length of the tissue.

All antibodies and staining reagents are described in Table S1 and Table S2. Histology was imaged using either a Nikon Eclipse E600 with a Q-Imaging Retiga Exi camera or a Nikon Eclipse NI-E Fluorescence Upright microscope coupled to a Zyla sCMOS camera (Andor Technology).

Western blots

Western blots were performed essentially as described [53]. Ears were harvested and the epidermis was isolated by incubating skin in distilled water at 60 °C for 20 seconds and then in ice cold PBS for 20 seconds before the epidermis was gently scraped off. Epidermal sheets were then lysed on ice with a Polytron PT 10-35 tissue homogenizer in lysis buffer (50 mM Tris-HCl pH 7.7, 1% Triton-X, 150 mM NaCl, 1 mM EDTA, 10 mM NaF, 5 mM β-glycerophosphate, 2 mM $NaVO_3$, 1 mM 1,10-ortho-phenanthroline (Sigma-Aldrich), and protease inhibitor cocktail set III (EMD Millipore)). Samples (10-15 µg protein) were separated on a 10% SDS-polyacrylamide gel, transferred to nitrocellulose paper, and Western blots were then stained as indicated. Antibody staining was detected using ECL Plus Western blotting substrate (Thermo Fisher Scientific). Blots were first stained for phosphoEGFR, stripped with 1 M Tris pH 6.75, β-mercaptoethanol, and SDS at room temperature followed by incubation at 60 °C, and then reprobed for total EGFR. All antibodies used for Western blots are described in Table S1 and Table S2. Western blots were quantified with ImageJ software and the ratio of phosphoEGFR: total EGFR was determined and normalized to the ratio of the control samples.

Epidermal permeability measurement

Toluidine blue dye penetrance was measured essentially as described [53]. Dehydrated and rehydrated ear skin was incubated for 2 min in 0.1% toluidine blue dye (Sigma-Aldrich) before destaining and toluidine blue dye extraction

with a solution of 2.5% H_2SO_4, 2.5% H_2O, and 95% methanol. Colorimetric values were measured at 620 nm and the total amount of toluidine blue dye was calculated using the volume of extraction solution, which was constant among the conditions.

In vitro experiments

Mouse keratinocyte-LC co-cultures:

Primary mouse keratinocyte cultures were prepared from mouse tail skin as described [53]. The isolated epidermal cells were plated in 8-well chamberslides (Lab-Tek) coated with 7 ng/μL collagen I (BD Biosciences) at 2-4 x 10^5 cells per well in serum-free keratinocyte growth media 2 (KGM2) (PromoCell). At 3-4 days later, keratinocytes were at 90% confluency and sorted LCs added at a density of 20,000-25,000 LCs per well. The co-cultures rested overnight and were then exposed to UVR and analyzed 24 hours later. Unless indicated, co-cultures were exposed to UVR in approximately 200 μL of minimally colored culture media containing 3.3 mM phenol red and without a plastic covering.

Keratinocyte EGFR knockdown co-cultures:

Primary mouse keratinocytes were cultured as described above and, at 40-50% confluency, were treated with control siRNA and two different EGFR siRNAs (siRNA #1 or #2) (Accell siRNA from Dharmacon, GE Lifesciences) according to the manufacturer's protocol. Target sequences of the siRNAs

were: siRNA #1- 5'-GAUUGGUGCUGUGCGAUUC-3' and siRNA #2- 5'-GCAUAGGCAUUGGUGAAUU-3'. The media was changed to normal keratinocyte growth media on day 4, and the co-culture experiments were subsequently conducted as described in Materials and Methods in the main text. Separate wells on the same chamberslides were collected on day 5 (the day of UVR exposure) to check efficiency of EGFR knockdown by flow cytometry.

Keratinocyte PD168393 treatment co-cultures:

Primary mouse keratinocytes were treated with 2 μM PD168393 (Cayman Chemicals), an irreversible EGFR inhibitor, for 30 minutes. The PD168393 was washed off with PBS and fresh keratinocyte growth media was supplied with or without LCs and the co-culture experiments were subsequently conducted. Keratinocytes from separate wells were collected at the time of co-culture and treated with EGF (200 ng/mL) to validate the efficiency of EGFR inhibition by measuring phosphoEGFR by flow cytometry.

Human keratinocyte-LC co-cultures:

Primary human keratinocytes (Lonza) were prepared according to the manufacturer's protocol and plated on collagen-coated chamberslides at 1-2 days before use. Human LCs and non-LC CD45+ cells were sorted from epidermis and added to 50-90% confluent keratinocyte cultures at 16,000-20,000 cells per chamberslide well. The co-cultures were rested overnight,

exposed to UVR, and examined 24 hours after UVR. Some wells of keratinocytes were treated with recombinant human HB-EGF (R&D Systems) at indicated concentrations, rested overnight, and then exposed to UVR. For anti-ADAM17 blocking experiments, LCs were pretreated with 200 nM of anti-human ADAM17 blocking antibody (Adipogen) or human IgG1 isotype control antibody (Adipogen) for 30 minutes before they were added with the antibodies to the keratinocytes. Anti-ADAM17 blocking antibody and IgG1 isotype control antibody was also included in keratinocyte cultures without LCs as additional controls.

Ex vivo ADAM17 activity assay by TNFR1 cleavage

Sorted mouse LCs were plated in a 96-well plate at 20,000-25,000 cells/well in RPMI 1640 supplemented with L-glutamine, penicillin/streptomycin, and HEPES buffer. The cells were treated with phorbol 12-myristate 13-acetate (PMA) (Sigma-Aldrich) at 25 ng/mL or UVR (500 J/m^2) and analyzed 45 minutes later. The cells were then stained with DAPI to exclude dead cells and for cell-surface TNFR1 (BioLegend). ADAM17 activity is expressed as the percent change in TNFR1 mean fluorescence intensity (MFI) relative to that of untreated LCs. Sorted human LCs (3,000-5,000 cells/well) were plated and treated with anti-ADAM17 blocking antibody or human IgG1 isotype control antibody for 30 minutes prior to UVR exposure and analysis of TNFR1 MFI.

EGFR ligand release assay with A431 indicator cells

A431 human squamous carcinoma cells (ATCC) were cultured according to the manufacturer's protocol in 96 well plates. At about 80% confluency, the A431 cells were serum-starved overnight then pretreated with 2 mM $NaVO_3$ for 15 minutes at 37° C, and were then treated with the conditioned supernatants from various cells for 10 minutes. The A431 cells were then collected and phosphoEGFR expression was measured by flow cytometry. All experiments were conducted with A431 cells in passage 2.

Lesion quantification

The remaining hair on the back skin of the mice was removed using Nair and photographs were taken. The total back area and lesional area (skin affected by erythema, scaliness, crustiness, or epidermal erosion) was measured by a blinded observer using ImageJ software and skin lesions were quantified as percent of back area.

mRNA quantification

Cells were sorted directly into RLT lysis buffer (Qiagen) with β-mercaptoethanol (Bio-Rad) and stored at -80°C until RNA extraction with Qiagen RNeasy Mini Kit. cDNA was generated using iScript cDNA synthesis kit (Bio-Rad) and real-time PCR was performed using iQ SYBR Green Supermix kit (Bio-Rad) on a Bio-Rad MyiQ thermal cycler or Maxima SYBR Green/ROX qPCR Master Mix (Thermo Fisher Scientific) on a StepOne Plus

Real-Time PCR system (Applied Biosystems). qPCR gene expression was quantified relative to *Gapdh*. Primer sequences used were:

Mouse (5'-3'):

Epgn forward: TGGGGGTTCTGATAGCAGTC, *Epgn* reverse: GGATCACCTCTGCTTCTTCG, *Egf* forward: CCTGGGAATGTGATTGCTTT, *Egf* reverse: CCTGGGAATTTGCAAACAGT, *Hbegf* forward: CCACCTCACTCCCTTTGTGT, *Hbegf* reverse: AAAGCTCCCTGCTCTTCCTC, *Tgfa* forward: AAGGCATCTTGGGACAACAC, *Tgfa* reverse: GCAGGCAGCTTTATCACACA, *Btc* forward: GGGTGTTTCCCTGCTCTGTA, *Btc* reverse: TGGATGAGTCCTCAGGTTCC, *Areg* forward: CATTATGCAGCTGCTTTGGA, *Areg* reverse: TTTCGCTTATGGTGGAAACC, *Ereg* forward: CGCTGCTTTGTCTAGGTTCC, *Ereg* reverse: GGGATCGTCTTCCATCTGAA, *Adam17* forward: GATGCTGAAGATGACACTGTG, *Adam17* reverse: GAGTTGTCAGTGTCAACGC, *Gapdh* forward: ATGTGTCCGTCGTGGATCTGA, *Gapdh* reverse: TTGAAGTCGCAGGAGACAACCT.

Human (5'-3'):

Epgn forward: ATGACAGCACTGACCGAAGAG, *Epgn* reverse: AACTGTCCAGTTACCTTGCTG, *Egf* forward: TCTCAACCCCTTGTACTTTGG, *Egf* reverse:

CAAGTCATCCTCCCATCACCA, *Hbegf* forward:

TTGTGCTCAAGGAATCGGCT, *Hbegf* reverse:

CAACTGGGGACGAAGGAGTC, *Tgfa* forward:

TCGTGAGCCCTCGGTAAGTA, *Tgfa* reverse:

GACTGGTCCCCCTTTCATGG, *Btc* forward: AAAGCGGAAAGGCCACTTCT, *Btc* reverse: AGCCTTCATCACAGACACAGG, *Areg* forward:

TGTCGCTCTTGATATCGGC, A*reg* reverse: ATGGTTCACGCTTCCCAGAG, *Ereg* forward: TACTGCAGGTGTGAAGTGGG, *Ereg* reverse:

GTGGAACCGACGACTGTGAT, *Adam17* forward:

TGATGAGCCAGCCAGGAGAT, *Adam17* reverse:

TATCAAGTCTTGTGGGGACAGC, *Gapdh* forward:

CGACAGTCAGCCGCATCTT, *Gapdh* reverse:

ATCCGTTGACTCCGACCTTC.

Skin histopathology scoring

A blinded expert dermatopathologist scored H&E stained sections based on dermal inflammation (0-3).

Human research participants

For immunofluorescence analysis, non-sun-exposed nonlesional skin from the buttocks of healthy controls and SLE patients was used. With the exception of one healthy control, all skin samples were from samples examined in [80]. Controls were between the ages of 28-65 and 67% were female. The SLE

patients met American College of Rheumatology criteria for SLE, were between the ages of 19-62 years old, and 79% were female. All SLE patients were currently receiving treatment at the time of the biopsy [80]. These samples were collected and used in accordance with the Institutional Review Board at the NYU School of Medicine.

For human LC and epidermal CD45+ non-LC cell isolation, human skin samples were collected from eight human patients undergoing elective reconstructive surgery at the Division of Plastic and Reconstructive Surgery at The Memorial Sloan Kettering Cancer Center (MSKCC). Seven of the eight patients were female and the patients were between the ages of 42-69 at the time of surgery. All tissue collection and research use adhered to protocols approved by the Institutional Review and Privacy Board at the Memorial Sloan Kettering Cancer Center, and all participants signed written informed consents.

Statistics

For all numerical comparisons, the distribution of the data was determined using the Shapiro-Wilkes test. For data that was normally distributed, the two-tailed unpaired Student's t-test was used to determine significance between two groups. For data that was not normally distributed, the nondirectional non-parametric Mann-Whiney *U* test was used to determine significance between

two groups. The statistical test and measure of uncertainty used for each figure is included in the figure legend.

REFERENCES

1. Lisnevskaia, L., Murphy, G. & Isenberg, D. Systemic lupus erythematosus. *The Lancet* **384**, 1878-1888 (2014).
2. Tsokos, G.C. Systemic lupus erythematosus. *The New England journal of medicine* **365**, 2110-2121 (2011).
3. Rahman, A. & Isenberg, D. Systemic lupus erythematosus. *The New England journal of medicine*, 929-939 (2008).
4. Jimenez, S., Cervera, R., Font, J. & Ingelmo, M. The Epidemiology of Lupus Erythematosus. *Clin Rev Allerg Immu* **25**, 3-11 (2003).
5. Fairweather, D., Frisancho-Kiss, S. & Rose, N.R. Sex differences in autoimmune disease from a pathological perspective. *The American journal of pathology* **173**, 600-609 (2008).
6. Aberer, E. Epidemiologic, socioeconomic and psychosocial aspects in lupus erythematosus. *Lupus* **19**, 1118-1124 (2010).
7. Hopkinson, N.D., Doherty, M. & Powell, R.J. Clinical features and race-specific incidence/prevalence rates of systemic lupus erythematosus in a geographically complete cohort of patients. *Annals of the rheumatic diseases* **53**, 675-680 (1994).
8. McCarty, D.J.*, et al.* Incidence of systemic lupus erythematosus. Race and gender differences. *Arthritis & Rheumatism* **38**, 1260-1270 (1995).
9. Tan, E.M.*, et al.* The 1982 revised criteria for the classification of systemic lupus erythrematosus. *Arthritis and Rheumatism* **25**, 1271-1277 (1982).
10. Yu, C., Gershwin, M.E. & Chang, C. Diagnostic criteria for systemic lupus erythematosus: A critical review. *Journal of Autoimmunity* **48-49**, 10-13 (2014).
11. Hochberg, M.C. Updating the American College of Rheumatology Revised Criteria for the Classification of Systemic Lupus Erythematosus. *Arthritis & Rheumatism* **40**, 1725-1734 (1997).
12. Fernandez, D. & Kirou, K.A. What Causes Lupus Flares? *Curr Rheumatol Rep* **18**, 14 (2016).
13. Tebbe, B.O.C.E. Epidemiology and socioeconomic impact of skin disease in lupus erythematosus. *Lupus* **6**, 96-104 (1997).
14. Gilliam, J.N. & Sontheimer, R.D. Distinctive cutaneous subsets in the spectrum of lupus erythematosus. *Journal of the American Academy of Dermatology* **4**, 471-475 (1981).
15. Provost, T.T. Nonspecific Cutaneous Manifestations of Systemic Lupus Erythematosus. in *Cutaneous Lupus Erythematosus* (eds. Kuhn, A., P., L. & Ruzicka, T.) 93-106 (Springer, 2004).
16. Patel, P. & Werth, V. Cutaneous lupus erythematosus: A review. *Dermatologic Clinics* **20**, 373-385 (2002).
17. Kuhn, a.*, et al.* Revised Cutaneous Lupus Erythematosus Disease Area and Severity Index (RCLASI): A modified outcome instrument for

cutaneous lupus erythematosus. *British Journal of Dermatology* **163**, 83-92 (2010).
18. Kuhn, A. & Landmann, A. The classification and diagnosis of cutaneous lupus erythematosus. *Journal of Autoimmunity* **48-49**, 14-19 (2014).
19. Kuechle, M.K. & Elkon, K.B. Shining light on lupus and UV. *Arthritis Res Ther* **9**, 101 (2007).
20. Chong, B.F. & Werth, V.P. Chapter 24 - Skin Disease in Cutaneous Lupus Erythematosus A2 - Wallace, Daniel J. in *Dubois' Lupus Erythematosus and Related Syndromes (Eighth Edition)* (ed. Hahn, B.H.) 319-332 (W.B. Saunders, Philadelphia, 2013).
21. Millard, T.P. & Hawk, J.L.M. Photosensitivity disorders: cause, effect, and management. *Am J Clin Dermatol* **3**, 239-246 (2002).
22. Rs, S. & Docken, W. An exacerbation of SLE after visiting a tanning salon. *JAMA* **255**, 3120-3120 (1986).
23. Schmidt, E., Tony, H.P., Bröcker, E.B. & Kneitz, C. Sun-induced life-threatening lupus nephritis. *Annals of the New York Academy of Sciences* **1108**, 35-40 (2007).
24. Kim, A. & Chong, B.F. Photosensitivity in cutaneous lupus erythematosus. *Photodermatology, photoimmunology & photomedicine* **29**, 4-11 (2013).
25. Kuhn, A., Wenzel, J. & Weyd, H. Photosensitivity, Apoptosis, and Cytokines in the Pathogenesis of Lupus Erythematosus: a Critical Review. *Clin Rev Allerg Immu*, 1-15 (2014).
26. Werth, V.P., Bashir, M. & Zhang, W. Photosensitivity in rheumatic diseases. *J Investig Dermatol Symp Proc* **9**, 57-63 (2004).
27. Golan, T.D., Elkon, K.B., Gharavi, A.E. & Krueger, J.G. Enhanced membrane binding of autoantibodies to cultured keratinocytes of systemic lupus erythematosus patients after ultraviolet B/ultraviolet A irradiation. *J Clin Invest* **90**, 1067-1076 (1992).
28. Reefman, E.*, et al.* Is disturbed clearance of apoptotic keratinocytes responsible for UVB-induced inflammatory skin lesions in systemic lupus erythematosus? *Arthritis Res Ther* **8**, R156 (2006).
29. Lichtenberger, B.M.*, et al.* Epidermal EGFR controls cutaneous host defense and prevents inflammation. *Sci Transl Med* **5**, 199ra111 (2013).
30. Raj, D., Brash, D.E. & Grossman, D. Keratinocyte apoptosis in epidermal development and disease. *J Invest Dermatol* **126**, 243-257 (2006).
31. Pasparakis, M., Haase, I. & Nestle, F.O. Mechanisms regulating skin immunity and inflammation. *Nat Rev Immunol* **14**, 289-301 (2014).
32. Kuhn, a., Krammer, P.H. & Kolb-Bachofen, V. Pathophysiology of cutaneous lupus erythematosus--novel aspects. *Rheumatology (Oxford, England)* **45 Suppl 3**, iii14-i16 (2006).
33. Steinman, R.M. & Cohn, Z.A. Identification of a novel cell type in peripheral lymphoid organs of mice. *J Exp Med* **137**(1973).

34. Banchereau, J. & Steinman, R.M. Dendritic cells and the control of immunity. *Nature* **392**(1998).
35. Doebel, T., Voisin, B. & Nagao, K. Langerhans Cells - The Macrophage in Dendritic Cell Clothing. *Trends Immunol*, 817-828 (2017).
36. Kashem, S.W., Haniffa, M. & Kaplan, D.H. Antigen-Presenting Cells in the Skin. *Annu Rev Immunol* **35**, 469-499 (2017).
37. Kaplan, D.H., Jenison, M.C., Saeland, S., Shlomchik, W.D. & Shlomchik, M.J. Epidermal langerhans cell-deficient mice develop enhanced contact hypersensitivity. *Immunity* **23**, 611-620 (2005).
38. Price, J.G.*, et al.* CDKN1A regulates Langerhans cell survival and promotes Treg cell generation upon exposure to ionizing irradiation. *Nat Immunol* **16**, 1060-1068 (2015).
39. Scholz, F., Naik, S., Sutterwala, F.S. & Kaplan, D.H. Langerhans Cells Suppress CD49a+ NK Cell-Mediated Skin Inflammation. *J Immunol* **195**, 2335-2342 (2015).
40. Sontheimer, R.D. & Pr, B. Epidermal Langerhans cell involvement in cutaneous lupus erythematosus. *J Invest Dermatol* **79**, 237-243 (1982).
41. Lemmon, M.A., Schlessinger, J. & Ferguson, K.M. The EGFR family: not so prototypical receptor tyrosine kinases. *Cold Spring Harb Perspect Biol* **6**, a020768 (2014).
42. Pastore, S., Mascia, F., Mariani, V. & Girolomoni, G. The Epidermal Growth Factor Receptor System in Skin Repair and Inflammation. *Journal of Investigative Dermatology* **128**, 1365-1374 (2008).
43. Ronan, T.*, et al.* Different Epidermal Growth Factor Receptor (EGFR) Agonists Produce Unique Signatures for the Recruitment of Downstream Signaling Proteins. *J Biol Chem* **291**, 5528-5540 (2016).
44. Nyati, M.K., Morgan, M.A., Feng, F.Y. & Lawrence, T.S. Integration of EGFR inhibitors with radiochemotherapy. *Nat Rev Cancer* **6**, 876-885 (2006).
45. Blobel, C.P. ADAMs: key components in EGFR signalling and development. *Nat Rev Mol Cell Biol* **6**, 32-43 (2005).
46. Li, X.*, et al.* iRhoms 1 and 2 are essential upstream regulators of ADAM17-dependent EGFR signaling. *Proc Natl Acad Sci U S A* **112**, 6080-6085 (2015).
47. Sahin, U. & Blobel, C.P. Ectodomain shedding of the EGF-receptor ligand epigen is mediated by ADAM17. *FEBS Lett* **581**, 41-44 (2007).
48. Sahin, U.*, et al.* Distinct roles for ADAM10 and ADAM17 in ectodomain shedding of six EGFR ligands. *J Cell Biol* **164**, 769-779 (2004).
49. Black, R.A.*, et al.* A metalloproteinase disintegrin that releases tumour-necrosis factor-alpha from cells. *Nature* **385**, 729-733 (1997).
50. Moss, M.L.*, et al.* Cloning of a disintegrin metalloproteinase that processes precursor tumour-necrosis factor-alpha. *Nature* **385**, 733-736 (1997).

51. El-Abaseri, T.B.*, et al.* Chemoprevention of UV light-induced skin tumorigenesis by inhibition of the epidermal growth factor receptor. *Cancer Res* **65**, 3958-3965 (2005).
52. El-Abaseri, T.B., Putta, S. & Hansen, L.A. Ultraviolet irradiation induces keratinocyte proliferation and epidermal hyperplasia through the activation of the epidermal growth factor receptor. *Carcinogenesis* **27**, 225-231 (2006).
53. Franzke, C.W.*, et al.* Epidermal ADAM17 maintains the skin barrier by regulating EGFR ligand-dependent terminal keratinocyte differentiation. *J Exp Med* **209**, 1105-1119 (2012).
54. Chia, J.J.*, et al.* Dendritic cells maintain dermal adipose–derived stromal cells in skin fibrosis. *J Clin Invest* **126**, 4331-4345 (2016).
55. Kumar, V.*, et al.* A dendritic-cell-stromal axis maintains immune responses in lymph nodes. *Immunity* **42**, 719-730 (2015).
56. Ivanov, S.*, et al.* CCR7 and IRF4-dependent dendritic cells regulate lymphatic collecting vessel permeability. *J Clin Invest* **126**, 1581-1591 (2016).
57. Astarita, J.L.*, et al.* The CLEC-2-podoplanin axis controls the contractility of fibroblastic reticular cells and lymph node microarchitecture. *Nat Immunol* **16**, 75-84 (2015).
58. Acton, S.E.*, et al.* Dendritic cells control fibroblastic reticular network tension and lymph node expansion. *Nature* **514**, 498-502 (2014).
59. Polla, L., Margolis, R., Goulston, C., Parrish, J.A. & Granstein, R.D. Enhancement of the Elicitation Phase of the Murine Contact Hypersensitivity Response by Prior Exposure to Local Ultraviolet Radiation. *J Invest Dermatol* **86**, 13-17 (1986).
60. Haratake, A.*, et al.* UVB-induced alterations in permeability barrier function: roles for epidermal hyperproliferation and thymocyte-mediated response. *J Invest Dermatol* **108**, 769-775 (1997).
61. Tamoutounour, S.*, et al.* Origins and functional specialization of macrophages and of conventional and monocyte-derived dendritic cells in mouse skin. *Immunity* **39**, 925-938 (2013).
62. Hohl, T.M.*, et al.* Inflammatory monocytes facilitate adaptive CD4 T cell responses during respiratory fungal infection. *Cell Host Microbe* **6**, 470-481 (2009).
63. Doerner, J.L.*, et al.* TWEAK/Fn14 signaling involvement in the pathogenesis of cutaneous disease in the MRL/lpr model of spontaneous lupus. *J Invest Dermatol* **135**(2015).
64. Iordanov, M.S.*, et al.* The UV (Ribotoxic) Stress Response of Human Keratinocytes Involves the Unexpected Uncoupling of the Ras-Extracellular Signal-Regulated Kinase Signaling Cascade from the Activated Epidermal Growth Factor Receptor. *Mol Cell Biol* **22**, 5380-5394 (2002).

65. Mascia, F.*, et al.* Genetic ablation of epidermal EGFR reveals the dynamic origin of adverse effects of anti-EGFR therapy. *Sci Transl Med* **5**, 199ra110 (2013).
66. Fry, D.W.*, et al.* Specific, irreversible inactivation of the epidermal growth factor receptor and erbB2, by a new class of tyrosine kinase inhibitor. *Proc Natl Acad Sci* **95**, 12022-12027 (1998).
67. Scheller, J., Chalaris, A., Garbers, C. & Rose-John, S. ADAM17: a molecular switch to control inflammation and tissue regeneration. *Trends Immunol* **32**, 380-387 (2011).
68. Horiuchi, K.*, et al.* Cutting edge: TNF-alpha-converting enzyme (TACE/ADAM17) inactivation in mouse myeloid cells prevents lethality from endotoxin shock. *J Immunol* **179**, 2686-2689 (2007).
69. Kaplan, D.H.*, et al.* Autocrine/paracrine TGFβ1 is required for the development of epidermal Langerhans cells. *J Exp Med* **204**, 2545-2552 (2007).
70. Bobr, A.*, et al.* Autocrine/paracrine TGF-beta1 inhibits Langerhans cell migration. *Proc Natl Acad Sci* **109**, 10492-10497 (2012).
71. Singh, B., Schneider, M., Knyazev, P. & Ullrich, A. UV-induced EGFR signal transactivation is dependent on proligand shedding by activated metalloproteases in skin cancer cell lines. *Int J Cancer* **124**, 531-539 (2009).
72. Ghoreishi, M. & Dutz, J.P. Murine models of cutaneous involvement in lupus erythematosus. *Autoimmunity Reviews* **8**, 484-487 (2009).
73. Kanauchi, H., Furukawa, F. & Imamura, S. Characterization of Cutaneous Infiltrates in MRL/1pr Mice Monitored from Onset to the Full Development of Lupus Erythematosus-Like Skin Lesions. *Journal of Investigative Dermatology* **96**, 478-483 (1991).
74. Menke, J.*, et al.* Sunlight Triggers Cutaneous Lupus through a CSF-1-Dependent Mechanism in MRL-Faslpr Mice. *The Journal of Immunology* **181**, 7367-7379 (2008).
75. Menke, J.*, et al.* Sunlight Triggers Cutaneous Lupus through a CSF-1-Dependent Mechanism in MRL-Faslpr Mice. *J Immunol* **181**, 7367-7379 (2008).
76. Eriksson, A.U. & Singh, R.R. Cutting edge: migration of langerhans dendritic cells is impaired in autoimmune dermatitis. *J Immunol* **181**, 7468-7472 (2008).
77. Morel, L.*, et al.* Genetic reconstitution of systemic lupus erythematosus immunopathology with polycongenic murine strains. *Proc Natl Acad Sci* **97**, 6670-6675 (2000).
78. Pisitkun, P.*, et al.* Autoreactive B cell responses to RNA-related antigens due to TLR7 gene duplication. *Science* **312**, 1669-1672 (2006).
79. Subramanian, S.*, et al.* A Tlr7 translocation accelerates systemic autoimmunity in murine lupus. *Proc Natl Acad Sci U S A* **103**, 9970-9975 (2006).

80. Izmirly, P.M.*, et al.* Dysregulation of the Microvasculature in Nonlesional Non-Sun-exposed Skin of Patients with Lupus Nephritis. *J Rheumatol* **39**, 510-515 (2012).
81. Monticelli, L.A.*, et al.* IL-33 promotes an innate immune pathway of intestinal tissue protection dependent on amphiregulin-EGFR interactions. *Proc Natl Acad Sci U S A* **112**, 10762-10767 (2015).
82. Arpaia, N.*, et al.* A Distinct Function of Regulatory T Cells in Tissue Protection. *Cell* **162**, 1078-1089 (2015).
83. Hatakeyama, M.*, et al.* Anti-Inflammatory Role of Langerhans Cells and Apoptotic Keratinocytes in Ultraviolet-B-Induced Cutaneous Inflammation. *J Immunol*, 2937-2947 (2017).
84. Cooper, K.D.*, et al.* UV exposure reduces immunization rates and promotes tolerance to epicutaneous antigens in humans: relationship to dose, CD1a-DR+ epidermal macrophage induction, and Langerhans cell depletion. *Proc Natl Acad Sci* **89**, 8497-8501 (1992).
85. Sontheimer, C., Liggitt, D. & Elkon, K.B. Ultraviolet B Irradiation Causes Stimulator of Interferon Genes–Dependent Production of Protective Type I Interferon in Mouse Skin by Recruited Inflammatory Monocytes. *Arthritis Rhematol* **69**, 826-836 (2017).
86. Kollias, N., Ruvolo, E., Jr. & Sayre, R.M. The value of the ratio of UVA to UVB in sunlight. *Photochem Photobiol* **87**, 1474-1475 (2011).
87. Uribe, P. & Gonzalez, S. Epidermal growth factor receptor (EGFR) and squamous cell carcinoma of the skin: molecular bases for EGFR-targeted therapy. *Pathology, research and practice* **207**, 337-342 (2011).
88. Shin, J.U., Park, J.H., Cho, B.C. & Lee, J.H. Treatment of epidermal growth factor receptor inhibitor-induced acneiform eruption with topical recombinant human epidermal growth factor. *Dermatology* **225**, 135-140 (2012).
89. Dubé, P.E.*, et al.* Epidermal growth factor receptor inhibits colitis-associated cancer in mice. *J Clin Invest* **122**, 2780-2792 (2012).
90. Dorner, T., Giesecke, C. & Lipsky, P.E. Mechanisms of B cell autoimmunity in SLE. *Arthritis Res Ther* **13**(2011).
91. Dorner, T., Jacobi, A.M. & Lipsky, P.E. B cells in autoimmunity. *Arthritis Res Ther* **11**(2009).
92. Der, E.*, et al.* Single cell RNA sequencing to dissect the molecular heterogeneity in lupus nephritis. *JCI Insight* **2**(2017).
93. Maney, S.K.*, et al.* Deletions in the cytoplasmic domain of iRhom1 and iRhom2 promote shedding of the TNF receptor by the protease ADAM17. *Science Signaling* **8**(2015).
94. Qing, X.*, et al.* iRhom2 regulates CSF1R cell surface expression and non-steady state myelopoiesis in mice. *Eur J Immunol* **46**, 2737-2748 (2016).
95. Aringer, M., Günther, C. & Lee-Kirsch, M.A. Innate immune processes in lupus erythematosus. *Clinical Immunology* **147**, 216-222 (2013).

96. Oke, V. & Wahren-Herlenius, M. Cutaneous lupus erythematosus: clinical aspects and molecular pathogenesis. *Journal of internal medicine* **273**, 544-554 (2013).
97. Reefman, E., Kuiper, H., Limburg, P.C., Kallenberg, C.G. & Bijl, M. Type I interferons are involved in the development of ultraviolet B-induced inflammatory skin lesions in systemic lupus erythaematosus patients. in *Ann Rheum Dis*, Vol. 67 11-18 (England, 2008).
98. Rönnblom, L. & Alm, G.V. The natural interferon-alpha producing cells in systemic lupus erythematosus. *Human immunology* **63**, 1181-1193 (2002).
99. Wenzel, J. & Tüting, T. Identification of type I interferon-associated inflammation in the pathogenesis of cutaneous lupus erythematosus opens up options for novel therapeutic approaches. *Experimental Dermatology* **16**, 454-463 (2007).
100. Wenzel, J., Zahn, S., Bieber, T. & Tüting, T. Type I interferon-associated cytotoxic inflammation in cutaneous lupus erythematosus. *Archives of Dermatological Research* **301**, 83-86 (2009).
101. Zahn, S.*, et al.* Ultraviolet light protection by a sunscreen prevents interferon-driven skin inflammation in cutaneous lupus erythematosus. *Experimental Dermatology* **23**, 516-518 (2014).